INFLUENCE OF EXTERNALLY INDUCED LATERAL AND PITCH VIBRATIONS ON THE PERFORMANCE OF FLEXIBLY MOUNTED ROTOR MECHANICAL SEALS

A Thesis

by

TRAVIS PUTNAM GREENSTREET

Submitted to the Office of Graduate and Professional Studies of
Texas A&M University
in partial fulfillment of the requirements for the degree of

MASTER OF SCIENCE

Chair of Committee,	Adolfo Delgado
Committee Members,	Steve Suh
	Chao Ma
Head of Department,	Guillermo Aguilar

December 2022

Major Subject: Mechanical Engineering

ABSTRACT

Mechanical seals are a form of dynamic sealing that have become an essential component in the operation of centrifugal pumps in industry. As mechanical seals are frequently seen to be the component with the shortest service life of those found in pumps, it is paramount to determine what conditions of operation impact their performance. Previous work has indicated that vibrations play a role in how seals perform during operation. Lateral vibrations specifically have been shown to diminish a mechanical seals service life, however the exact impact they have has yet to be determined. The work covered in this thesis strives to answer this question by externally exerting lateral vibrations upon an experimental system designed to simulate the operating conditions typical of industrial centrifugal pumps. Previous work has covered a cylindrical shape mode of motion, while this covers conical motion. The leakage of the seal is collected and measured between trials, while axial and lateral vibrations of the seal along with rotational torque and running speed are continually monitored and recorded. Leakage measurements and axial vibration measurements are used to evaluate the impact of the externally excited vibrations on the film thickness of the mechanical seal and are compared to previous test results. Lateral vibration measurements of the seal along with lateral vibration measurements of the rotor are evaluated based on their average vibration amplitudes change in behavior between different excitation frequencies and the magnitude of their response in the frequency domain. Lateral transmissibility of the rotating portion of the mechanical seal is evaluated based on the seal and rotor lateral vibration amplitudes. The measured torque and running speed are used to determine the power consumption of the seal and to determine whether there is a dependence on either chamber pressure or frequency. Leakage, axial vibration, lateral transmissibilty, and power consumption are used to quantify the mechanical seal's performance and determine whether externally induced lateral/pitched vibrations are of any consequence to the seal's operation. Power consumption and leakage are found to be independent of the excitation frequency. The average film thickness is found to decrease with the excitation frequency. The transmissibilty is found to be impacted by the externally induced lateral vibrations

as well, however contradictions in the results prevents to establish a correlation between the two variables.

DEDICATION

To my parents, Brad and Jinks Greenstreet, for the love, support, and guidance they have provided me all of my life. The best parts of myself I owe to them.

ACKNOWLEDGMENTS

I would like to thank my group of friends from my undergrad, for helping me to get my first degree and supporting me while I worked through my second.

I would like to thank the members of the Reliability & Performance group, Seung-Hyeop Hyun, Sean McClean, Brianna Johnson, Surya Balaji, and Anthony Dudlo for being not only essential team members, but friends throughout my time at the Turbomachinery Lab. A special thanks to Marie Kasprzyk, for being a friend, team member, and mentor to me.

I would like to Carl Johnson of the Turbomachinery Laboratory, for finding time to help with the many problems I encountered through my time in graduate school.

I would like to thank my sister, Natalie Shaw, and her husband, Ray Shaw, for all of the love and support they have provided me through my time at university.

I would like to thank my sister, Jessica Brooks, and her husband, Joshua Brooks. Jessi inspired me to become an engineer and Josh inspired me to go further.

I would like to thank Clay Norrbin, for designing and constructing the facilites used for this thesis and continually providing assistance throughout testing.

I would like to thank my committee members, Dr. Steve Suh and Dr. Chao Ma, for providing their feedback and support on this thesis work.

Finally, I would like to thank my graduate advisor, Dr. Adolfo Delgado, for providing the resources and facilities necessary to complete the work covered in this thesis, but more importantly, for seeing the student I was and believing in the engineer I would become, I could not have asked for a better mentor.

CONTRIBUTORS AND FUNDING SOURCES

Contributors

The principal investigator for this work is Dr. Adolfo Delgado. The test rig was initially constructed by a former student, Clay Norribin, who has continued to provide support on the testing covered in this thesis. This work is supported by a thesis committee consisting of Dr. Adolfo Delgado and Dr. Steve Suh of the Department of Mechanical Engineering and Dr. Chao Ma of the Department of Engineering Technology and Industrial Distribution.

All other work conducted for the thesis was completed by the student independently.

Funding Sources

The test rig's initial commissioning was supported by the Turbomachinery Research Consortium, Dr. Adolfo Delgado, and Dr. Dara Childs. The student's graduate study has been supported by TechnipFMC and Dr. Adolfo Delgado.

NOMENCLATURE

FMR	Flexibly Mounted Rotor
VFD	Variable Frequency Drive
PID	Proportionanl-Integral-Derivative
DE	Drive End
NDE	Non-Drive End
Ra	Roughness Average
RPM	Rotations Per Minute
OEM	Original Equipment Manufacturer
EOM	Equation of Motion
T_L	Lateral Transmissibilty
A_s	Seal Ring Lateral Amplitude of Vibration
A_r	Rotor Lateral Amplitude of Vibration
ω	Motor Rotational Speed
P	Power Consumption
T_f	Torque due to Friction
T_s	Torque due to Sliding at the Seal Interface
T_d	Torque due to Fluid Drag
r_s	Sliding Radius of the Seal
P_c	Contact Pressure
A_{int}	Seal Interface Area

TABLE OF CONTENTS

Page

LIST OF FIGURES

FIGURE Page

LIST OF TABLES

TABLE Page

1. INTRODUCTION

Mechanical Seals are a form of dynamic sealing commonly found in rotating machinery, specifically in applications that require high rotor speed and high pressure in the system [1]. The exact configuration of a mechanical seal varies widely between applications, but the basic design consists of two rings with faces manufactured to a high tolerance of flatness and installed parallel with one another to allow for full contact. One of the faces is mounted to some stationary portion of the system, commonly referred to as the stator, while the other is mounted to the shaft, also known as the rotor, with one or both of the faces being flexibly fixed to its housing by having springs positioned on the back of the ring [2]. The seals typically have at least one face being made of a ceramic, with the other face almost always being a carbon-graphite composite due to a need for high abrasion resistance, although metals are sometimes used for specific applications [3]. Figure 1.1 provides a visual representation of a typical mechanical seal configuration with the stationary portion being the flexibly mounted face.

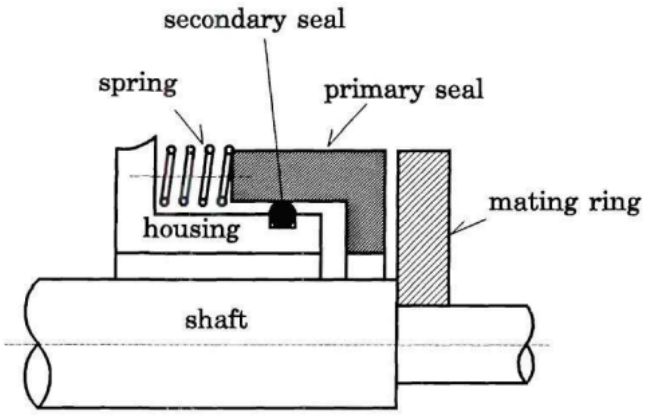

Figure 1.1: Drawing of a mechanical seal flexibly mounted stator detailing its main components, reprinted from [4]

This design comes together to form a seal when a pressure differential is created across the faces of the seals. When a certain pressure differential is achieved, the sealed hydraulic pressure can overcome the closing force of the springs and the opposing hydraulic pressure to open up a gap between the seal faces, allowing a fluid film to form [2], as illustrated in Figure 1.2.

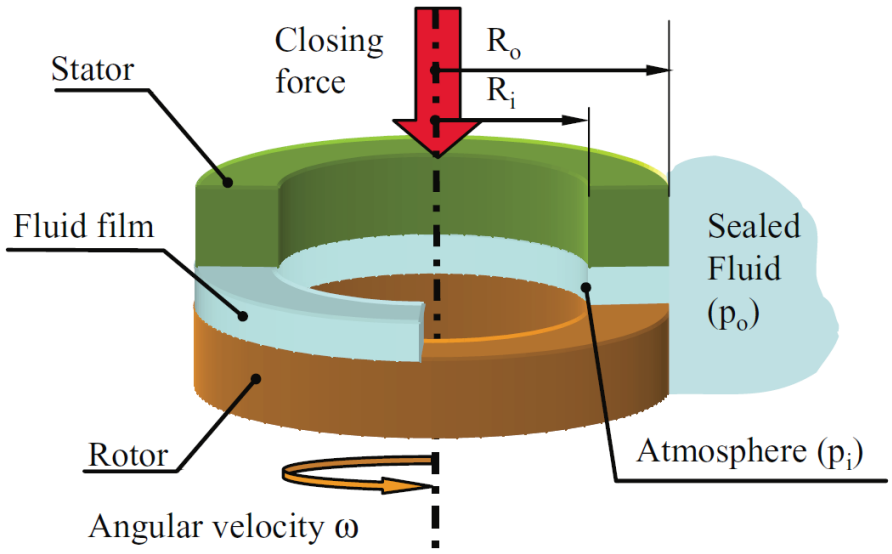

Figure 1.2: Partial cut-view of a mechanical seal depicting the fluid film layer formed between the seal faces, reprinted from [5]

The formation of this fluid film prevents the seals from experiencing excessive wear and thus greatly extends their service life. As a consequence of this method of lubrication, mechanical seals do leak, however this amount managed by controlling the geometry of the seals, the operating pressure differentials and speed of the system, the fluid properties, and by minimizing external effects[6].

Most industrial pumps rely on mechanical seals to minimize process fluid leakage. Seal failures can lead to reduced performance and pump (system-level) failures. One of the most common factors leading to reduction in mechanical seal service life is excessive vibrations in pumps operating outside of their specified operating range [7]. Axial vibration in the rotor is already known

to be one of the major causes of failure for mechanical seals operating in pumps [8], however little work has been done on analyzing the effect of lateral vibrations. In 2005, Stefanko and Leishear[9] investigated mechanical seal failures and concluded that a reduction of lateral vibrations increases the life of the seals. This finding has lead to the development of a test rig at Texas A&M University capable of inducing lateral vibrations on a rotor and observing its effect on the operation of mechanical seals.

The goal of this thesis is to evaluate the impact of externally induced lateral/pitch vibrations on the dynamic response and performance of mechanical seals when the shaft experiences a conical shape mode of motion. An FMR mechanical seal operates in a test rig that simulates typical mechanical seal operating conditions, specifically those of a centrifugal pump. Operating conditions, including vibration frequency and chamber pressure, were varied while monitoring the response of the rotating component of the seal and leakage rate. The processed data is used to quantify parameters of performance in the form of leakage, film thickness, lateral transmissibility, and power consumption to evaluate the impact of external vibrations on seal performance.

2. LITERATURE REVIEW

The following section provides an overview of the progression of mechanical seal experimentation highlighting the increasing need for evaluating the effect of vibration on the seal performance.

The first known mechanical seal design was created in 1903 by George Cook with the purpose of being used for a centrifugal compressor refrigeration application[10]. This design was soon applied to centrifugal pumps, which with the aforementioned compressors, would drive the desire for advancement of mechanical seals. Earlier designs of mechanical seals used dissimilar materials, with a trend suggesting a desire to pair soft or flexible materials with a hard and stiff face made of a metal or plastic. Going into the 1950s mechanical seals became much closer to what they are today with developing industries such as aerospace pushing for the need to have higher quality materials in the faces such as the carbon-based ceramics typically seen in modern seals[10].

Some of the earliest experimental work done on mechanical seals was done in 1961 by Denny [11] to study the pressures in the gap between the two sealing faces. The separation between the seal faces was monitored during trials and the wear that propagated across trials was observed. This results of this experiment allowed Denny to conclude that vibration of the rotor influenced the performance of the seals regarding the pressure they experienced in between the faces, however the wear the seals experienced was not attributed to this.

In 1982, Etsion [12] conducted a review of testing done on mechanical seals, noting that vibration had become an issue for mechanical seal operation in the previous two decades. The testing done since Denny's experiments by Metcalfe had resulted in the discovery that three modes of seal operation exist: a stable mode, which exhibits vibration at the same frequency as the shaft's rotation, a transition mode, and an unstable mode which experiences uncontrolled vibration [13]. Despite this advancement and others Etsion reviewed, he found that at this point in time no research had been done on mechanical seals with regards to their behavior in a dynamic setting.

In 1984, Etsion and Constantinescu [14] tested the dynamic behavior of a cone-face non-contacting mechanical seal with a flexibly mounted stator, which based on his previously discussed

review, could very well be the first non-steady testing done on mechanical seals. Motion of the stator was observed through the means of three proximity probes and was used to track the relative misalignment between the stator and rotor. All three of the aforementioned modes of vibration that can be experienced during seal operation were tested, with the stable mode seeming to dominate at low to moderate speeds. It was found that the misalignment between the rotor and stator is time dependent and that this relative misalignment can be a source of seal failure.

In 1989, Green [15] developed a closed-form solution for the response of a flexibly mounted rotor to misalignment that can exist in a rotordynamic system and compared its performance to that of a flexibly mounted stator. Misalignment in this situation is the relative offset between the rotor and stator, and is a common issue that results due to manufacturing and assembly tolerances and is directly impacted by the system's parameters and operating conditions. The analysis conducted suggested that an FMR seal provides superior performance to that of an FMS seal based on the observed parameters such as the dynamic transmissibilty and the maximum relative misalignment.

In 1995, Lee and Green [16] tested the dynamic behavior of a non-contacting mechanical seal with a flexibly mounted rotor. This experiment was focused on showing that shaft flexibility is made significant by its own rotation and examining how changing this assumption effects the performance of the mechanical seal due to the lateral vibration it would introduce. The shaft in this system was designed to be particularly stiff, however it is worth noting that it was cantilevered, which may have increased flexibility, a complete overview of this system can be seen in Figure 2.1.

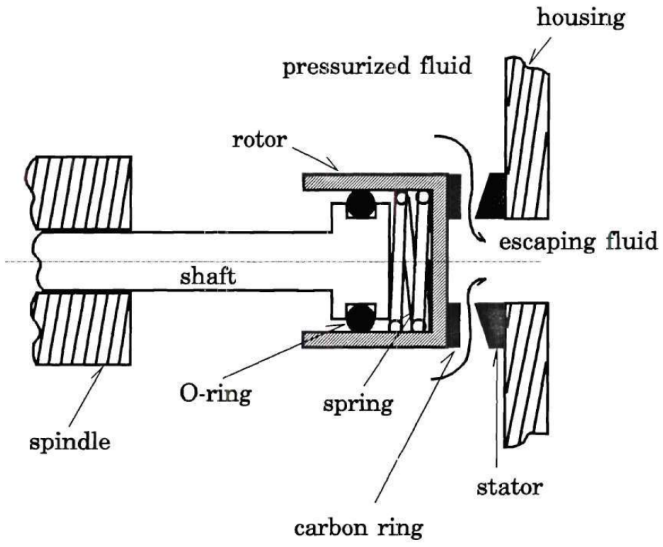

Figure 2.1: Model of a non-contacting FMR seal test rig, reprinted from [16]

The results of this testing did in fact indicate a harmful effect of the flexibility of the shaft on the dynamics of the seal, even at relatively low operating speeds.

In 2005, Stefanko and Leishear [9] conducted a series of experiments within a centrifugal pump to demonstrate a relationship between the service life of mechanical seals and the vibration they experienced. Several different cases were tested to display the impact of different system parameters on the vibration, these included controlling the operating speed, altering the bearing design, and changing the stiffness of the pump. Multiple failures of mechanical seals were observed in

their experiments and vibrations were thought to be the culprit. As previously mentioned, they concluded that minimizing lateral vibrations on a mechanical seal was important for increasing its service life.

In 2017, Varney and Green [17] presented a model for mechanical seal dynamics that is coupled with the rotordynamics of the system in which the seal is operating. The model takes both faces (stationary and rotating) to be flexibly mounted and allowed to experience angular, axial, and eccentric deflection. This model is valid for both steady-state and dynamic operation. The importance of this model is its ability to take the vibrations of the system into account when evaluating the performance of mechanical seal, as previous models have treated seals and their rotordynamic system as independent entities.

In 2018, Norrbin and Childs [18] presented results of a model for predicting the stability and response of a flexibility mounted rotor mechanical seal. Within the model, the seal is externally excited with lateral vibrations through the rotor housing. Figure 2.2 displays a schematic of the system represented in the model.

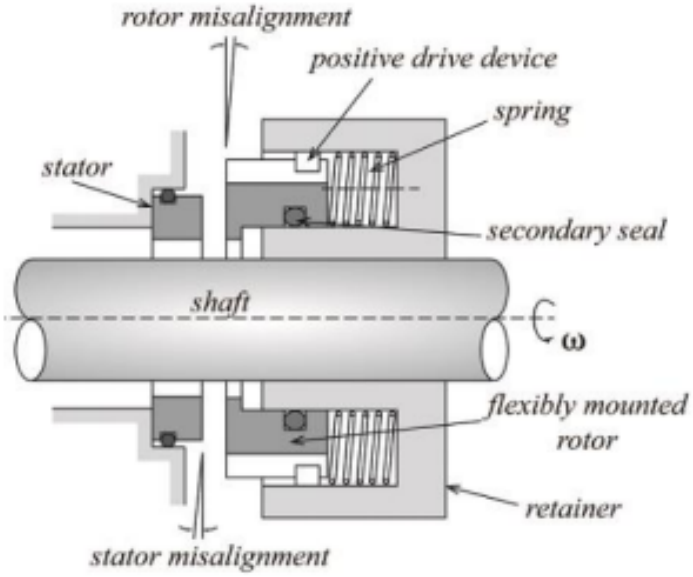

Figure 2.2: Model of a non-contacting FMR seal test rig, reprinted from [18]

The seal's response is represented through the transmissibility and its stability is represented through the damping ratio. Both the damping ratio and the transmissibility were found to be dependent on the external excitation frequency and the running speed of the shaft. A critical region with exceptionally high transmissibility was found when the damped natural frequency, running speed, and excitation frequency are equivalent.

In 2020, Norribin and Delgado [19] presented results from experiments conducted on an FMR seal that involved external lateral vibrations. This is the same test rig used in the current experimental work and it is described in detail in the next section. The system was excited at the midspan of the shaft assembly to induce a cylindrical mode of motion and the relative displacement of the rotating seal in relation to the stationary was measured. The wobble of the mechanical seal was found to remain constant with the level of external excitation, indicating a lack of dependence of response on lateral vibrations.

For at least the past seventy years mechanical seals have been suspected to be impacted by the vibrations produced by the machine they operate within. Etsion[12] noticed the lack of experimental work covering this and completed what could be the first test done on seals in a dynamic setting. Stefanko and Leishear[9] noted that lateral vibrations do indeed have an impact on the longevity of mechanical seals, implying that it would also effect their performance. Norribin[19] presented results on how a mechanical seal performs with lateral vibrations that induce a cylindrical mode of motion upon the rotor. The next step is to observe how the same seal performs under the next mode of vibration, the conical mode.

3. EXPERIMENTAL FACILITIES AND TESTING

3.1 Test Rig

The test rig used for the experimental work covered in this thesis was designed by Clay Norbin [19]. The mechanical seal test rig is able to simulate a typical running pump environment a mechanical seal may operate in. Figure shows 3.1 a broad view of the entire experimental setup.

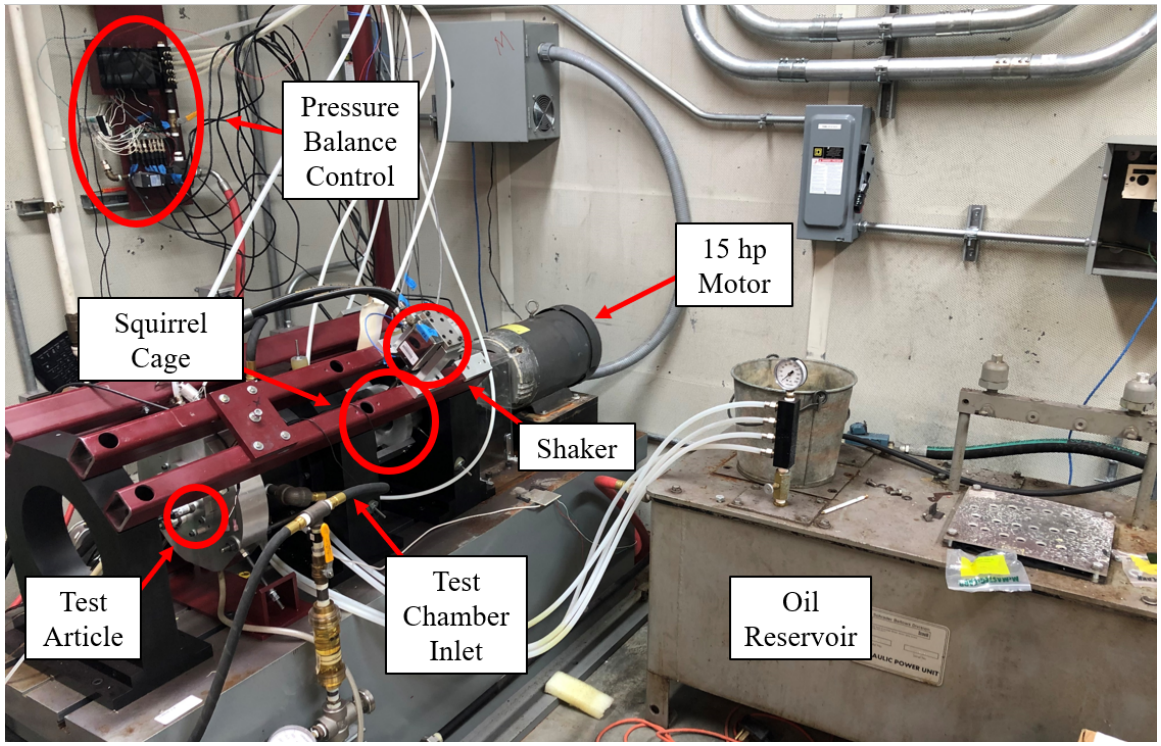

Figure 3.1: Externally vibrated mechanical seal experimental setup

The test rig is capable of housing one FMR mechanical seal with a maximum radius of 76 mm and pressurizing the test article up to at least 125 psi with possibility of going up to 200 psi in its current configuration. A detailed overview of the components of the test rig is covered in Figure 3.2

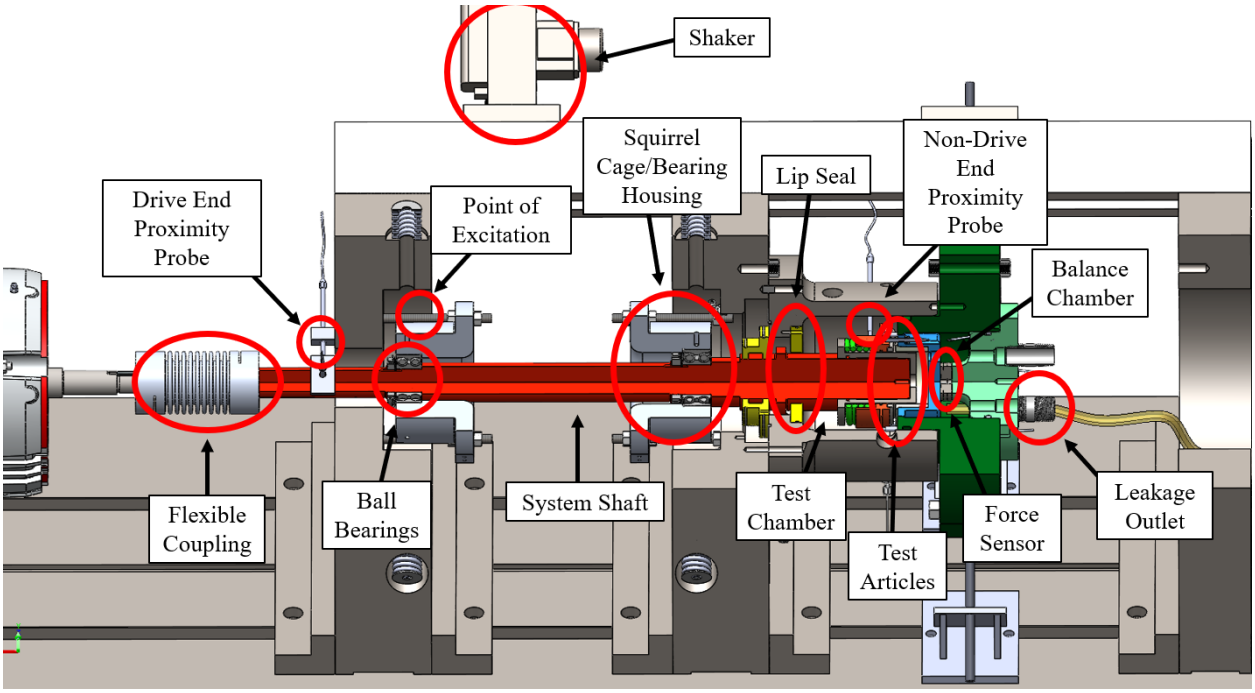

Figure 3.2: Test rig cutout view

Rotor motion is measured at the Drive-End near the flexible coupling seen on the left of Figure 3.2, while the Non-Drive End is measured next to the test article. Ball bearings support the shaft and are located within the squirrel cages, one of which is the point at which the stingers connect to the rotor to induce the conical mode of vibration. A lip seal separates the test chamber from the bearings and the outside environment. The force sensor is located on the Non-Drive end of the stationary seal face next to the balance chamber. The system shaft runs through the entire assembly. The actual test article is located between the balance chamber and the test chamber.

An image of the inside of the seal chamber with the rotating ring still in place can be seen in Figure 3.3.

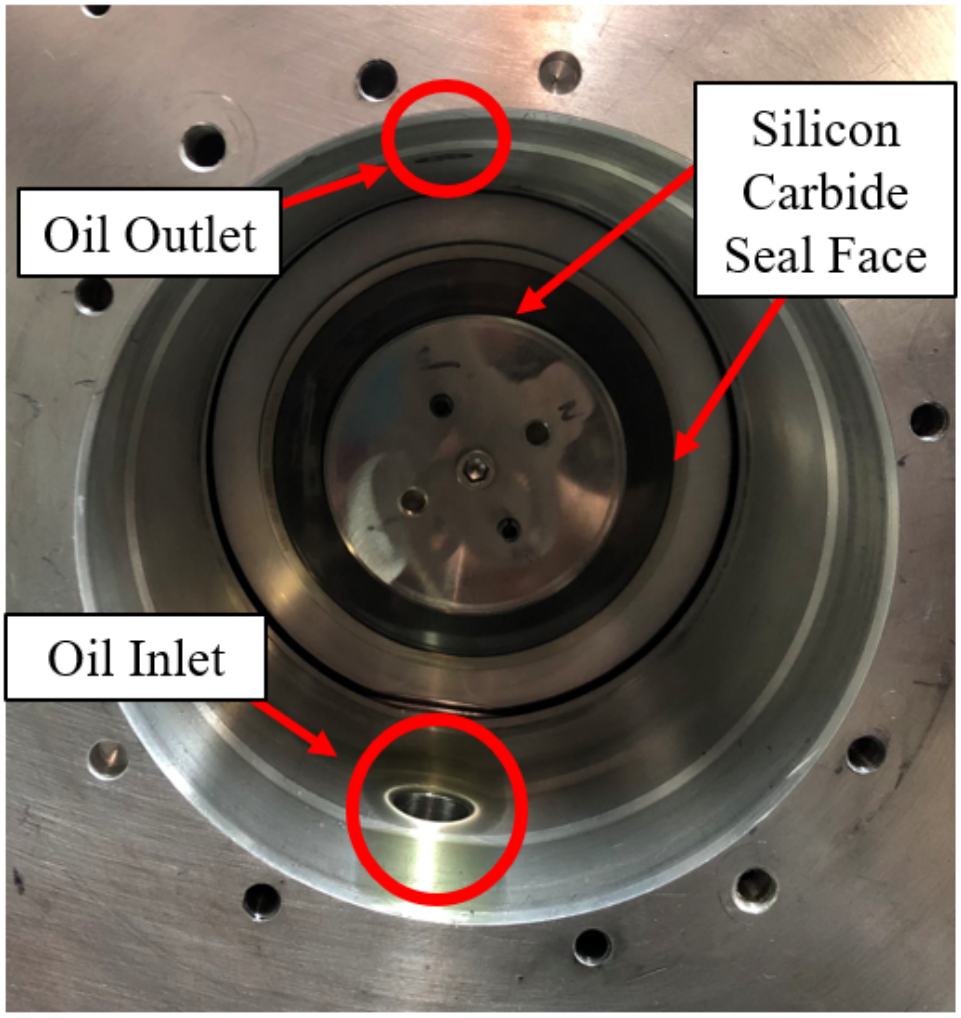

Figure 3.3: Test chamber inside view depicting seal face and oil ports

The rotating seal housing has an OD of 60 mm on the NDE that drops down down to 32 mm on its back side. This allows for clearance so that it can freely float on its flexible mounts and respond to the external excitation.

The stationary seal housing is equipped with five proximity probes to monitor the response of the rotating seal relative to that of the fixed stationary seal. Figure 3.4 shows these probes in place.

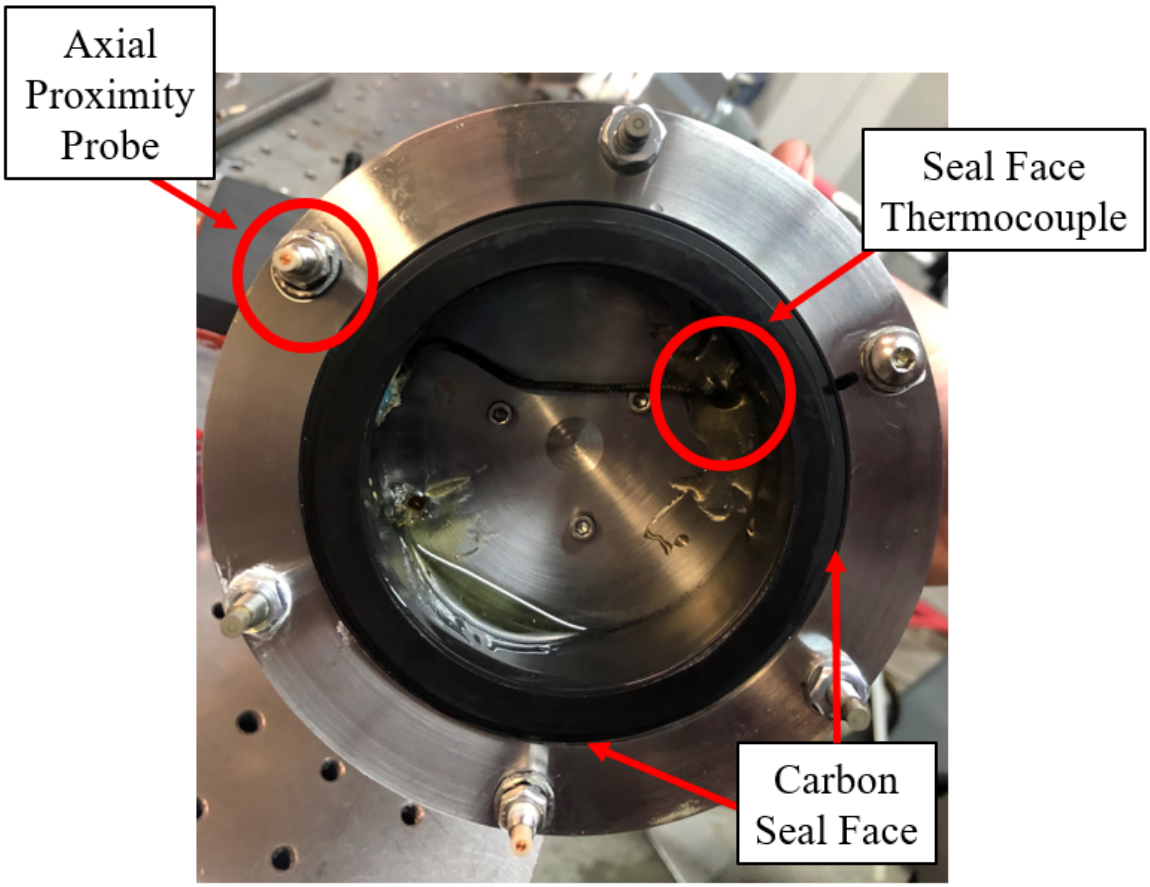

Figure 3.4: Stationary seal housing with prox probes

These axial sensors, along with two additional radial probes track the mechanical seal's five degrees of freedom in real time. Furthermore, a force sensor located on the rear of the stationary housing monitors load and torque in all three directions on the stationary face.

ISO-VG2 mineral oil is used as the process fluid and is sealed from a volume of ambient air. An exit chamber with an outlet port is located on the side of the seals with ambient pressure and leakage from this chamber is collected in an external container. The flow loop is a modified API plan 54 with a gear pump capable of reaching 32 lpm and 200 psi. A DC motor with a VFD con-

troller drives the pump supplying oil to the test chamber from an external reservoir. A cooling loop and an electric heater control the temperature of the fluid in the system.

A balance chamber provides a reactionary thrust to the axial load of the pressurized test chamber protects the shaft assembly and leaves the seal face reactionary forces unaffected. The balance chamber is supplied with shop air that is regulated through the use of a feedback PID controller that automatically adjusts the air supply. The thrust measured in the axial direction on the stationary seal is used by the PID controller as the feedback necessary to adjust the supply pressure. Figure 3.5 is a diagram representing the closed feedback loop that governs the operation of the balance chamber.

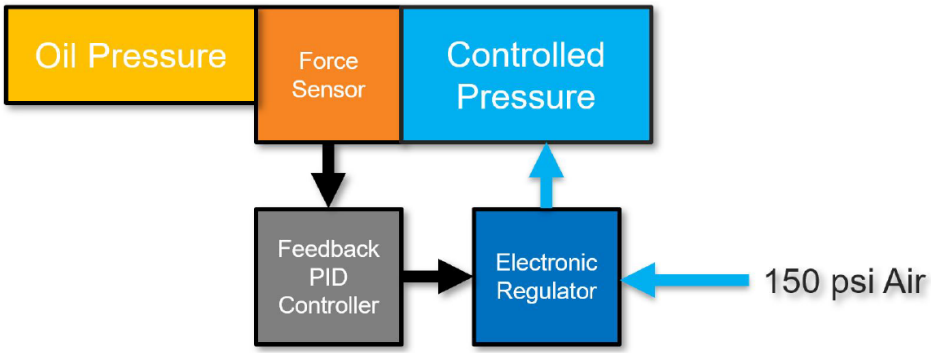

Figure 3.5: Balance chamber PID feedback loop, reprinted from [19]

The external vibrations needed for testing are generated by a pair of electro-hydraulic shakers that are mounted perpendicular to the rotor and 90° apart from one another. Figure 3.6 displays one of the shakers.

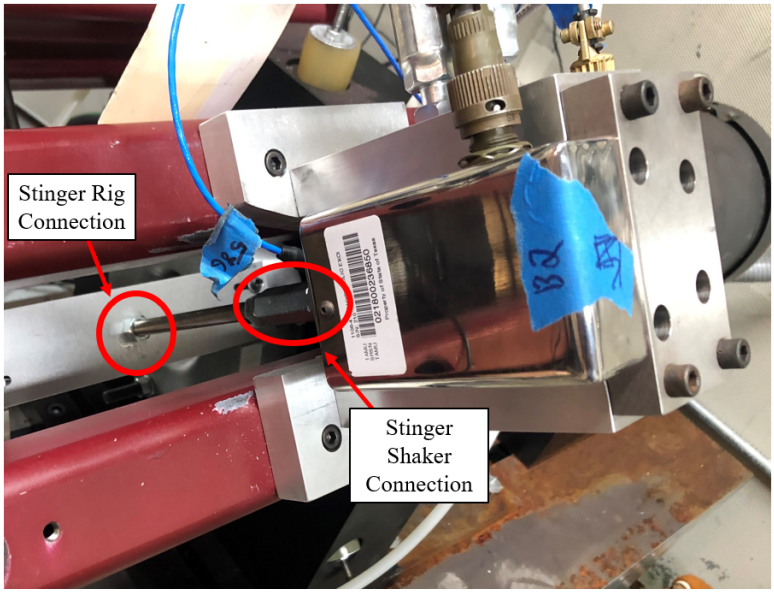

Figure 3.6: Electro-Hydraulic shaker

Their orthogonal orientation with one another allows for a uniform whirling motion of the FMR assembly during testing. Slender threaded rods (stingers) connect each of the shakers to the squirrel cage and transfer lateral force while minimizing any concentrated moments. Figure 3.7 depicts the location of one of the stingers.

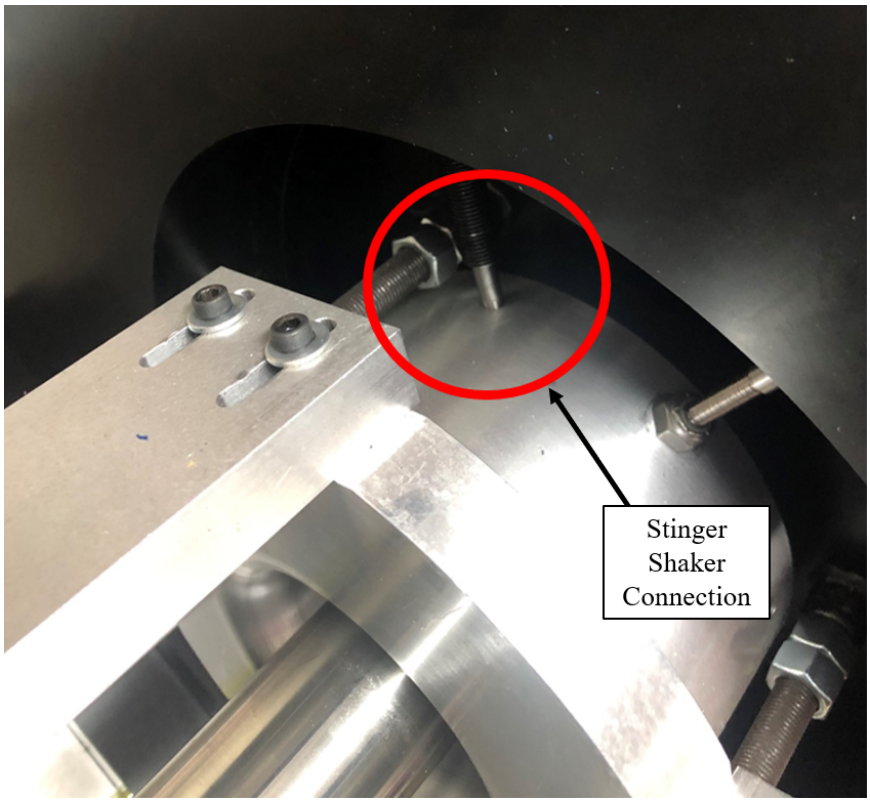

Figure 3.7: Electro-Hydraulic stinger connection to squirrel cage

These connections allow for the shakers to pitch the shaft and create conical motion for the mechanical seal. A 15 hp DC motor drives the shaft through a flexible coupling with a relatively low lateral stiffness of 337 N/mm that effectively decouples the motor dynamic forces from the rest of the system.

3.2 Test Article

The mechanical seal used during testing was designed by a major mechanical seal manufacturer, Flowserve, to represent a seal that would typically be found in industry. Figure 3.8 shows the entire seal assembly, the red curve indicates where the faces contact.

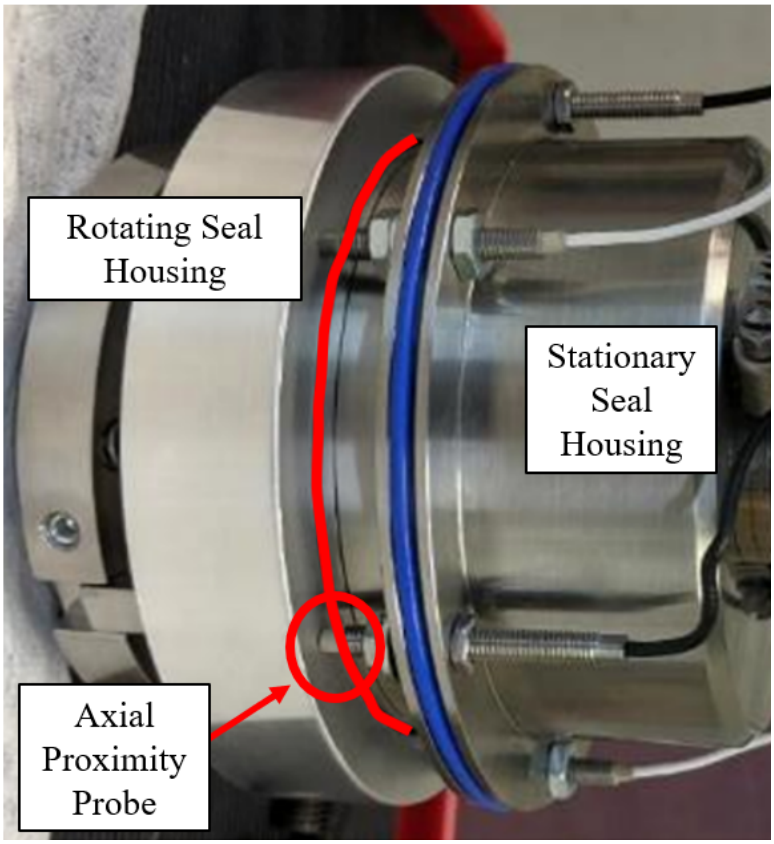

Figure 3.8: Test article rotating and stationary components mated at the faces

As previously mentioned, the test article is an FMR mechanical seal with an ID of 75 mm and a mass of 0.96 kg. The seal is a standard hard-soft material configuration with the rotating face being made of a hard silicon carbide and the stationary face a soft carbon. Figures 3.9 and 3.10 shows the rotating and stationary seal faces respectively.

Figure 3.9: Rotating seal

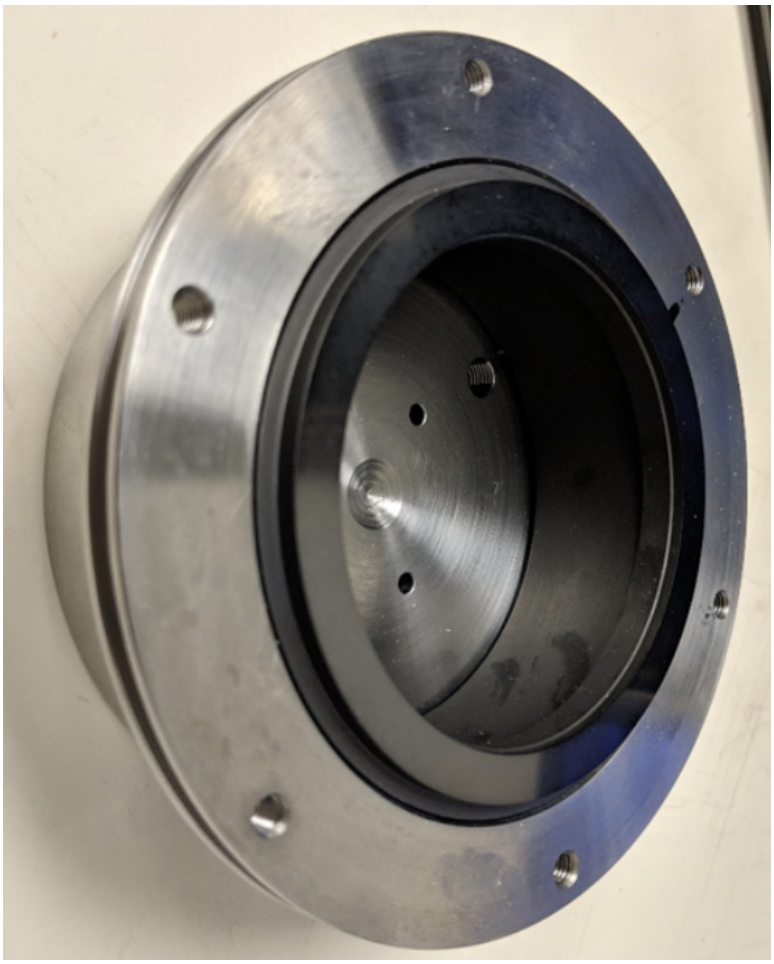

Figure 3.10: Stationary seal

The stationary seal surface roughness was measured to have an Ra of 70 nm prior to testing with a stylus based profilometer. The rotating seal was analyzed with an optical profilometer and found to have an Ra of approximately 65 nm.

3.3 Test Procedure

Table 3.1 outlines the tests conducted, with pressure and excitation frequency as the independent experimental variables. The excitation frequencies were chosen to be fractions of the running speed, 1/8, 1/4, and 1/2 of 58.3 Hz. The pressures are similar to those included in previous testing[19].

Table 3.1: Test Matrix Listing Test Parameters

Trial	**Pressure(psig)**	**Frequency(Hz)**
1A	30	0
1B	30	7.2
1C	30	14.5
2A	30	29
2B	50	0
2C	50	7.2
3A	50	14.5
3B	50	29
3C	100	0
4A	100	7.2
4B	100	14.5
4C	100	29

Testing starts with building up to the desired trial pressure by controlling the amount of oil flow that diverts into the test chamber vs the amount of flow that flows through a bypass line within the flow loop. This is done through the use of a gate valve with a pressure gauge located near the test chamber as shown in Figure 3.11.

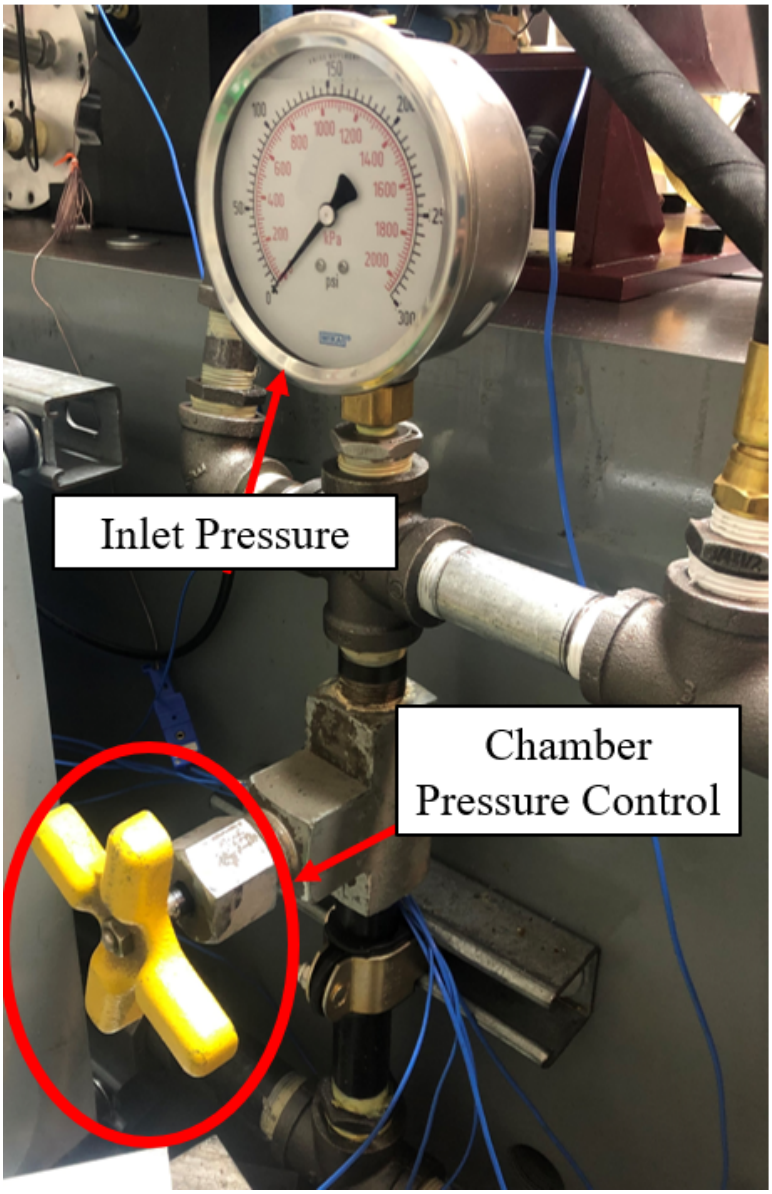

Figure 3.11: Chamber pressure control valve

This pressure is built slowly to allow for the PID controller to effectively balance the axial thrust by supplying the adequate amount of air pressure. The flow rate of the oil to the seal chamber is monitored with a flowmeter and is kept at 1.6 - 1.7 gpm for each trial. After the chamber pressure is stabilized at the current trial value the motor is set to ramp up to 3500 rpm over an interval of 60 seconds. This speed represents the typical running speed of centrifugal industrial pumps after accounting for slippage. The motor speed is monitored in real time via an optical tachometer shown in Figure 3.12.

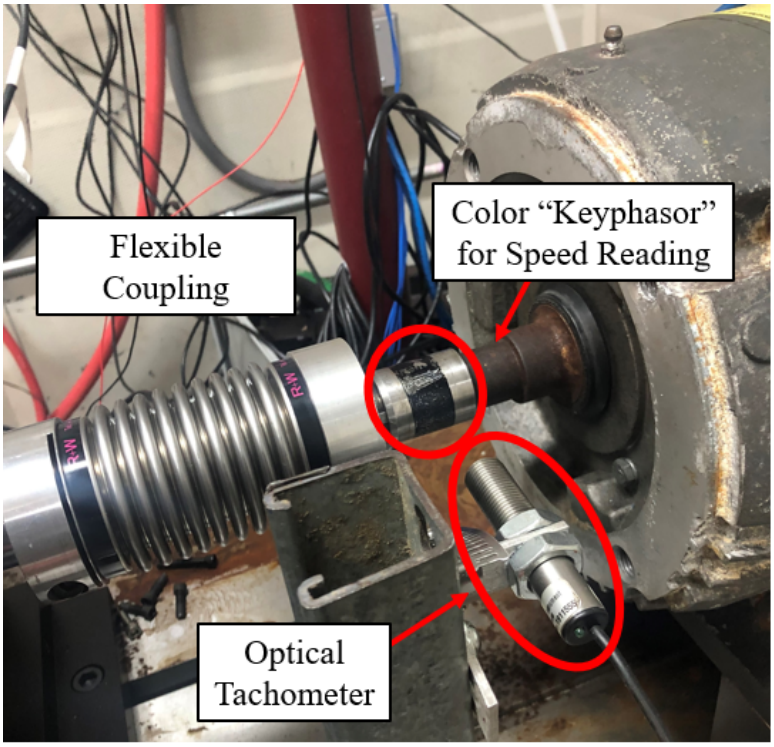

Figure 3.12: Optical tachometer reading flexible coupling connection to 15 hp motor

A reflective piece of tape that is bonded to the shaft acts as a color "Keyphasor". After the motor reaches full speed, the temperatures of the test chamber and the stationary seal face are monitored until they reach a steady value. Steady state is considered to be when the temperature changes by less than a degree Fahrenheit over the course of five minutes.

Once steady state is achieved, the baseline trial without shaking begins. The leakage container, seen in Figure 3.13, is emptied of any residual oil and weighed on a scale with a precision of +/- 0.1 g.

Figure 3.13: Leakage collection container

The container is then connected to the leakage outlet line from the test chamber and a twenty minute timer is set to measure the trial length. 25 second snapshots of all the sensor readings are collected at the beginning, middle, and end of each trial. After the trial time is reached, the leakage container is weighed again and the difference in weight is divided over the twenty minute trial length to acquire the average leakage rate. After the baseline test is completed, the shakers are attached and set to shake with a dynamic load of 1000 N(240 lbf) at the current trial's excitation frequency. The leakage measurements are repeated for each subsequent trial until the entire pressure set is completed.

Torque about the rotor axis, the seal and rotor lateral vibration, and relative axial vibration between the seal faces are monitored throughout each trial for quantifying the seal performance.

4.1 Mechanical Seal Leakage

In order to have a reasonable service life, mechanical seals require a fluid film between their faces to allow for lubrication and cooling. This lubrication film results in mechanical seals leaking, however the factors that effect the leakage are known and their impact can be characterized with Equation 4.1[6].

$$\dot{m} = r_0 \int_0^{2\pi} \rho(-\frac{h^3}{12\mu}\frac{\partial p}{\partial r})d\theta \tag{4.1}$$

This relationship is based upon the assumptions that a hydrodynamic film exists between the two faces, that the flow is laminar and that the fluid system can be modeled as flow through a radial annular gap[2]. $\dot{m}$ represents the mass flow rate of the leakage through the seal faces, r_0 represents the outside radius of the seal face, h represents the thickness of the film between the two seal faces, p represents pressure, μ represents the dynamic viscosity of the fluid running across the seal face, and ρ represents the density of the fluid. Figure 4.1 visualizes the coordinates r and θ's relationship to the geometry of the seal.

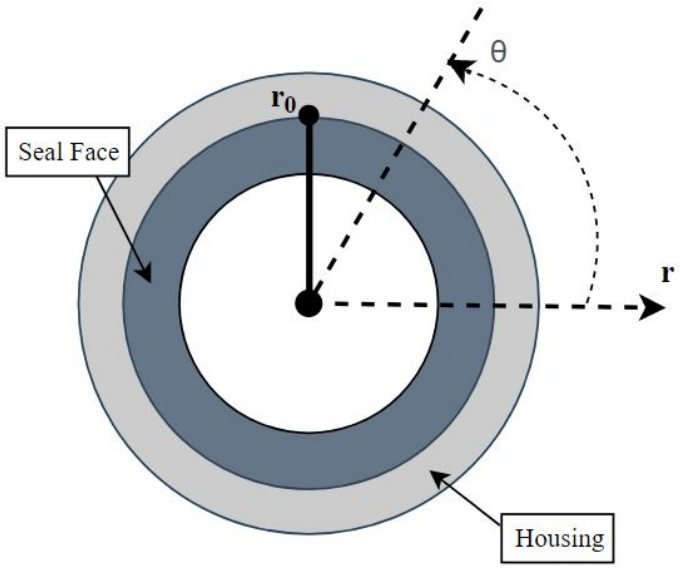

Figure 4.1: Leakage equation coordinates

This function provides insight into what system parameters need to be considered in order to understand, and more importantly, control the leakage in a mechanical seal. Both density and viscosity are physical characteristics of the lubricant being used in concert with the mechanical seal that, at first glance, have opposite effects on the leakage. These properties are both temperature dependent for a given fluid, so the temperature of the working fluid needs to be controlled. The radius of the component is directly proportional to leakage so while there are certainly situations needing larger seals, minimizing this will be something that needs to be considered in the design process. A large differential in pressure also increases leakage.

The last variable within this relation, the film thickness, is influenced by multiple system parameters. Film thickness is affected by the seal face geometry and the average face roughness, illustrating the need for high precision machining and stiff materials that resist deformation. Film thickness is also a function of the relative surface velocity of the two seal faces, so a higher operating speed will typically result in a larger amount of leakage. Finally, the net axial force on the mechanical seal, the force generated by the pressure differential, will also effect the leakage, as a higher amount of closing force will limit the amount the seal opening during operation. This has an

interesting effect on seal performance as a higher pressure differential supposedly will create more leakage for the seal, however depending on the effective area on either side of the seal that the two pressure are applied, there is the possibility for situations where a higher pressure differential can actually result in a lower amount of leakage. This design feature is called "pressure compensation".

Previous testing on the performance of mechanical seals has been conducted at Texas A&M University. This testing was focused more on the performance of a specific set of mechanical seals with relation to the pressure and rotational speed they were experiencing. This testing did not include external vibrations and focused solely on the leakage and power consumption of the mechanical seals. A model of the test rig used for this experimental work can be seen in Figure 4.2.

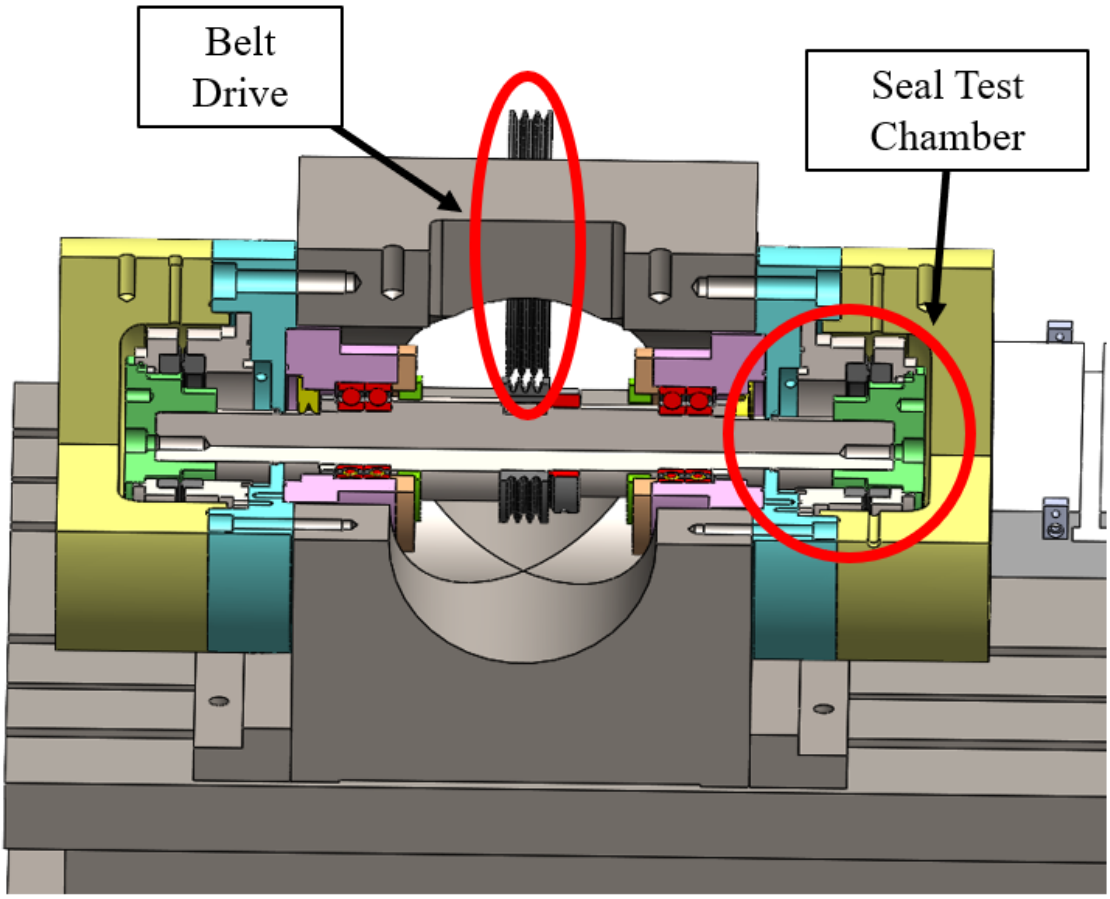

Figure 4.2: Texas A&M mechanical seal test rig

This setup differs from the rig used for dynamic testing in that it houses much larger seals, 8.25" OD, and is symmetrically balanced. It also lacks any sensors for measuring vibrations, only having the instrumentation necessary to monitor motor speed and torque and the process fluid temperature. Figure 4.3 shows some of the results from these tests.

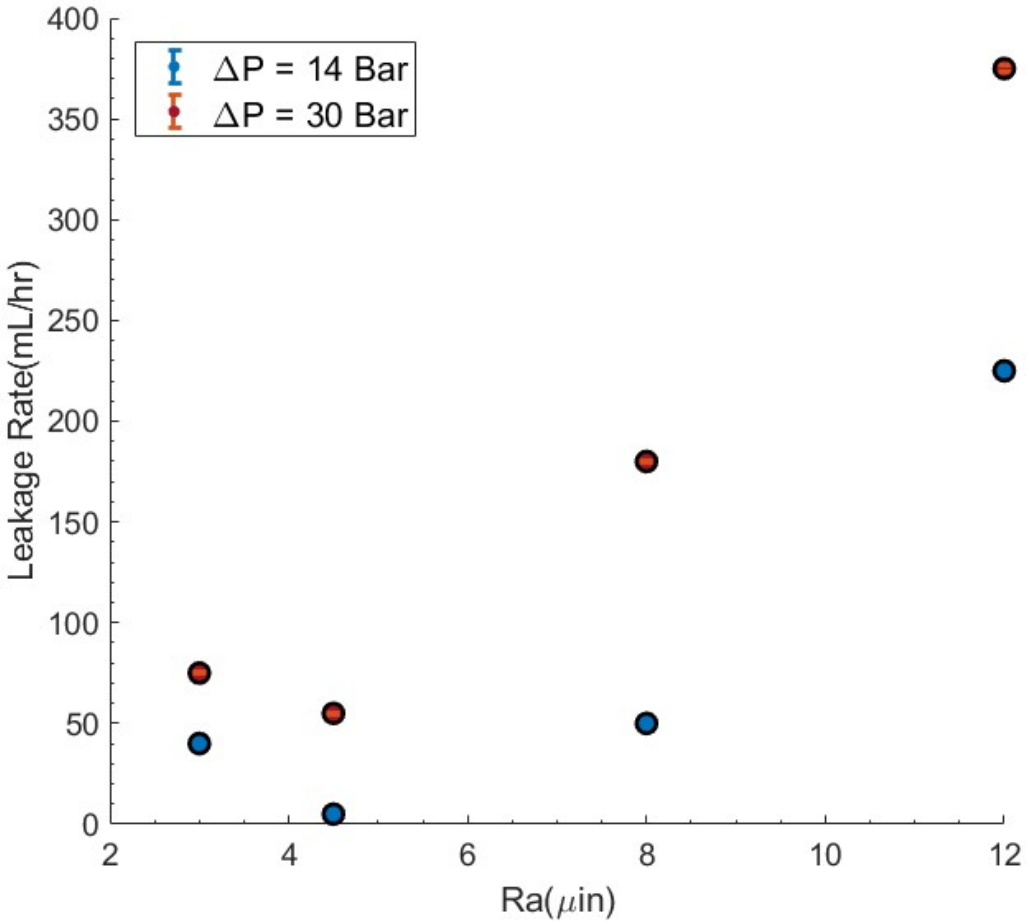

Figure 4.3: Mechanical seal leakage results

The trials pertaining to this specific set of data were performed with a consistent running speed, the same fluid that ran at a steady temperature for the duration of the trial, and one mechanical seal that showed an increasing level of roughness through continued testing. The minimum and maximum data roughness points were expected leakage results at those pressures provided by

the seal manufacturer. As all of the other parameters that affect leakage are held constant for these results, this data serves to provide insight into how the pressure differential and the seal face roughness can effect seal leakage. An increase in average roughness over the mechanical seal face generates more leakage through the seal, suggesting that rougher seal faces have thicker films. Furthermore, Figure 4.3 shows that there is indeed a higher amount of leakage for a greater pressure differential, as the 30 Bar pressure differential has a significantly higher leakage rate than the 14 Bar leakage at all of their corresponding roughness trials.

While these tests provide an overall understanding of the system parameters that influence the seal performance, these experimental results do not include the effects of external factors. One of these factors is the vibrations of the machine and this will be further explored in the next section.

4.2 Influence of Vibrations

Mechanical seals are constantly subject to vibrations during operation of pumps, therefore it is important to understand the impact vibrations have on mechanical seal performance. Axial vibrations can certainly be said to have an impact on the film thickness between the faces and thereby effect their performance. The influence of lateral vibrations is a topic that has only been explored in a theoretical sense. Norrbin and Childs [18] developed a model aimed at analyzing the impact a pump's vibration has on an FMR seal's dynamics.

Varney and Green's[17] model on how a pump's vibration influence an FMR seal's dynamics found that if the mechanical seal is 1/10th the mass of the rotor it will influence the rotordynamics of the system. The seal used for the research covered in this thesis has a mass of 0.96 kg[19] while the rotor has an approximate mass of 9.78 kg, meaning this system falls within that threshold. Norrbin and Childs[19] developed a model based off an EOM for the FMR seal's lateral displacement and pitch and a model of internal damping created by Childs[20]. The model assumes that the o-ring between the rotating seal and the rotor has a frequency dependent stiffness and damping, as well as the system, with its dynamic coefficients also having a speed dependence. However, the film thickness of the mechanical seal is assumed to frequency independent.

Predictions from the model showed that the vibration of the pitch for the rotating seal is related to the lateral vibration of the rotor. These two values are coupled by the axial distance between the center of the o-ring and the center of inertia of the seal ring, meaning that aligning the centers of these two components axially will remove any coupling. The transmissibility of the system is also predicted, in order to quantify the response of the seal under different operating conditions. Lateral transmissibility is defined as the ratio of the amplitude of lateral vibration of the seal ring over the amplitude of lateral vibration of the rotor. For the measurements taken in this research, the NDE response corresponds with the lateral vibration of the seal and the DE response corresponds with the rotor lateral vibrations. The lateral transmissibility can be expressed as follows in Equation 4.2.

$$T_L = \frac{A_s}{A_r} \tag{4.2}$$

This equation, along with other components of the model were used to determine the transmissibility factor depending on whether the seal itself or the rotor has internal damping. Figure 4.4 shows contour plots of the predicted transmissibility at different possible conditions[20].

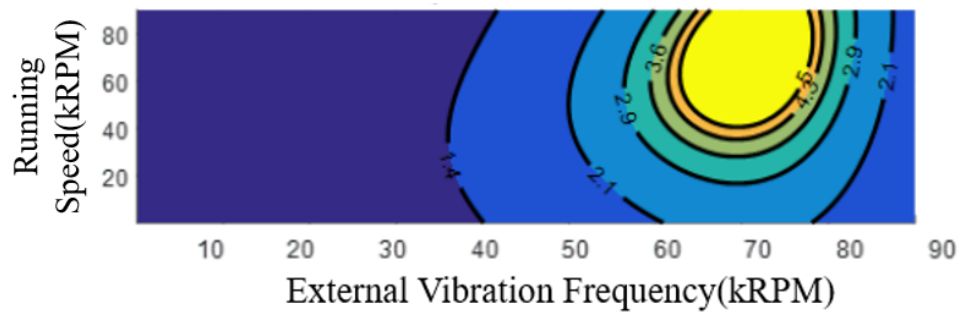

(a) Transmissibility with full internal damping

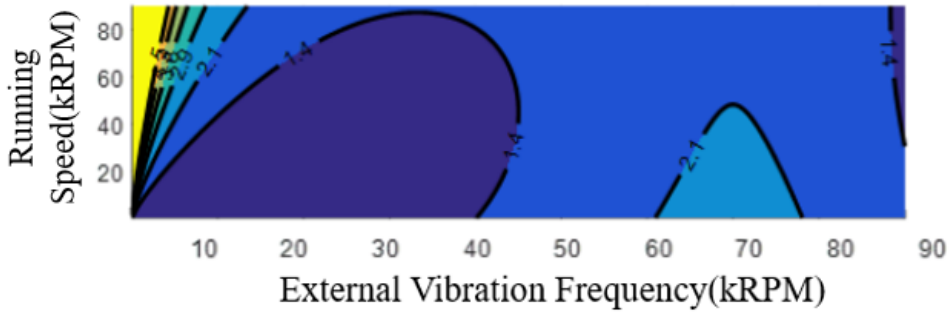

(b) Transmissiblity with no seal internal damping

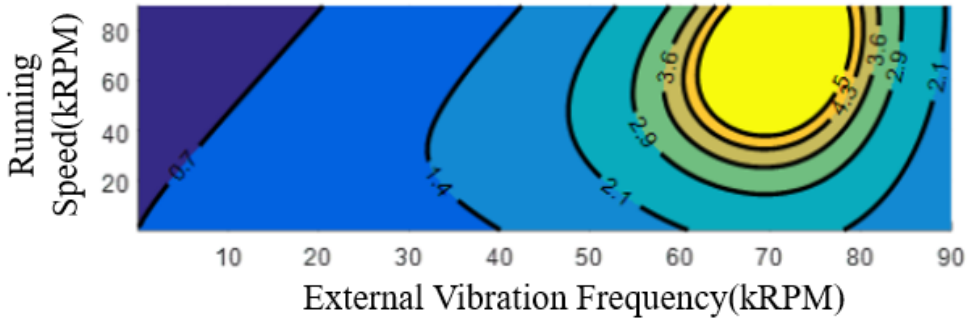

(c) Transmissiblity with no rotor internal damping

Figure 4.4: Transmissibility vs. running speed vs. excitation frequency[20]

The operating parameters listed in Table 3.1 coupled with the results discussed in the next section could provide insight into what conditions the system experiences during testing. From Figure 4.4b, sub-synchronous excitation displays a particularly high level of transmissibility when the internal damping of the seal ring is assumed to be zero, while Figures 4.4a and 4.4c show that with internal damping the seal only experiences an exceptionally high response around an excitation and running speed of 70 kRPM. These predictions show that the transmissibility and thus the performance of the seal is expected to be speed and frequency dependent. Processing and analyzing the data collected for this thesis will serve to evaluate this model.

5. RESULTS AND DISCUSSION

The performance of this mechanical seal will be quantified in the following section through the leakage, film thickness, transmissibilty, and power consumption. Uncertainty is representative of the accuracy of the associated sensor and the standard deviation of a trials distribution when averaging results.

5.1 Leakage and Film Thickness

A total of twelve trials were ran for this experiment with three different pressure and four different levels of excitation(one being no excitation). Leakage from the mechanical seal was collected for each trial and an average leakage rate for the duration of that trial was estimated based on the weight of the leakage and the length of the trial. The leakage rate for each pressure related to the trial excitation can be seen in Figure 5.1. Each set of data points is denoted by a pressure differential to allow for comparison to the previous leakage results in Figure 4.3, and to align with the theory discussed in the previous section. Since the oil was sealed from an ambient volume, this pressure differential is equivalent to the chamber pressure.

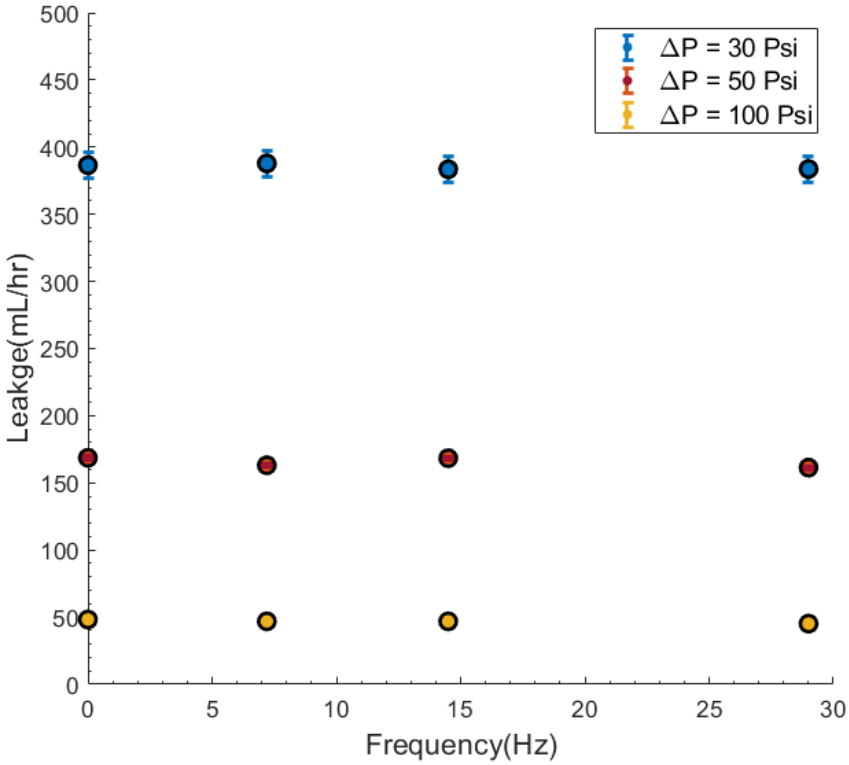

Figure 5.1: Mechanical seal leakage rate vs. excitation frequency at different test pressures

These results clearly show that the excitation frequency does not have a noticeable impact on the leakage the mechanical seal experiences. There is no significant change in the leakage rate across the different excitation frequencies for each pressure. However, what does have an impact on the leakage is the pressure differential across the seal. A higher pressure shows a decrease in the amount of leakage that passes through the mechanical seal, which is contradictory to the results seen in Figure 4.3 and what would be expected from Equation 4.1. As the geometry of the seal remained constant between trials the only other possible factors that could have created this result are a reduction in film thickness or an increase in the kinematic viscosity of the oil. Both of these can be evaluated with other parameters that were recorded during testing.

While the viscosity of the process fluid was not directly measured during testing, the data collected can be used to infer this parameter between trials. Kinematic viscosity for lubricants

is a function of temperature and decreases as the temperature of the fluid increases [21]. The temperature of the fluid within the chamber was measured for each trial and from this, the trend of the viscosity can be inferred. Figure 5.2 shows the average chamber temperature measured during testing for the three trial pressures.

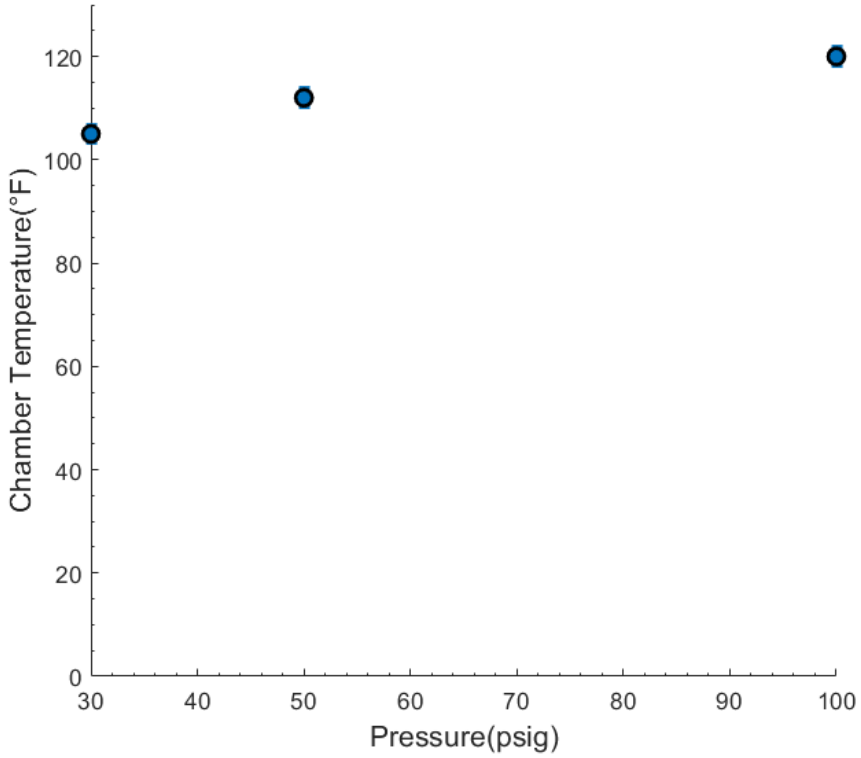

Figure 5.2: Chamber temperature vs. pressure

The temperature of the chamber, and therefore the process fluid, slightly increases with the pressure over testing. An increase in temperature would suggest a decrease in viscosity which should actually increase leakage. Furthermore, the change in temperature is relatively small and would likely not yield a large enough change in viscosity to have a major impact either way on the leakage.

The relative axial displacement between the rotating and stationary seals was measured during

testing. These measurements are not the exact film thickness, however they can still be used to show how the film thickness behaves under different conditions as the axial gap readings are simply the film thickness with an offset that would remain constant throughout testing. It is also worth noting that thermal expansion can effect these readings, but considering the minor changes in temperature between pressures seen in Figure 5.2, the effect here would be negligible. Figure 5.3 shows the average axial gap reading for each pressure when there is no excitation frequency.

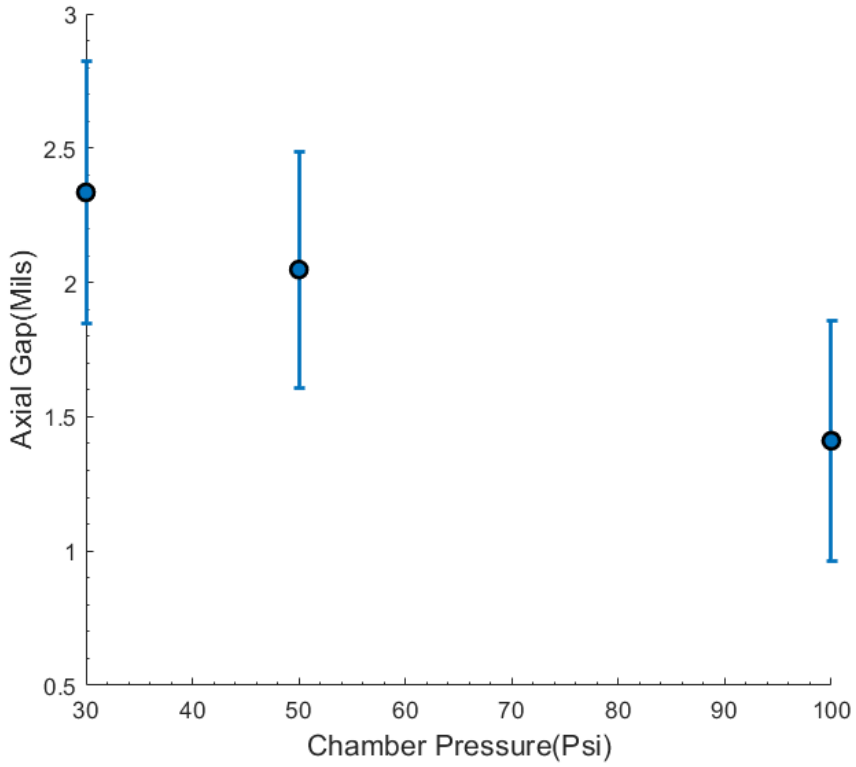

Figure 5.3: Average axial gap vs. chamber pressure without external excitation

This data shows a downward trend in the average axial gap with an increase in the chamber pressure. While a change in 0.0003 in. may seem trivial, a mechanical seal of this size would be expected to have a film thickness on the order of 10^{-4} in.[6]. From this, it is clear that the film thickness decreases with a higher chamber pressure. This trend can further be observed with the

external lateral vibrations as shown in Figure 5.4.

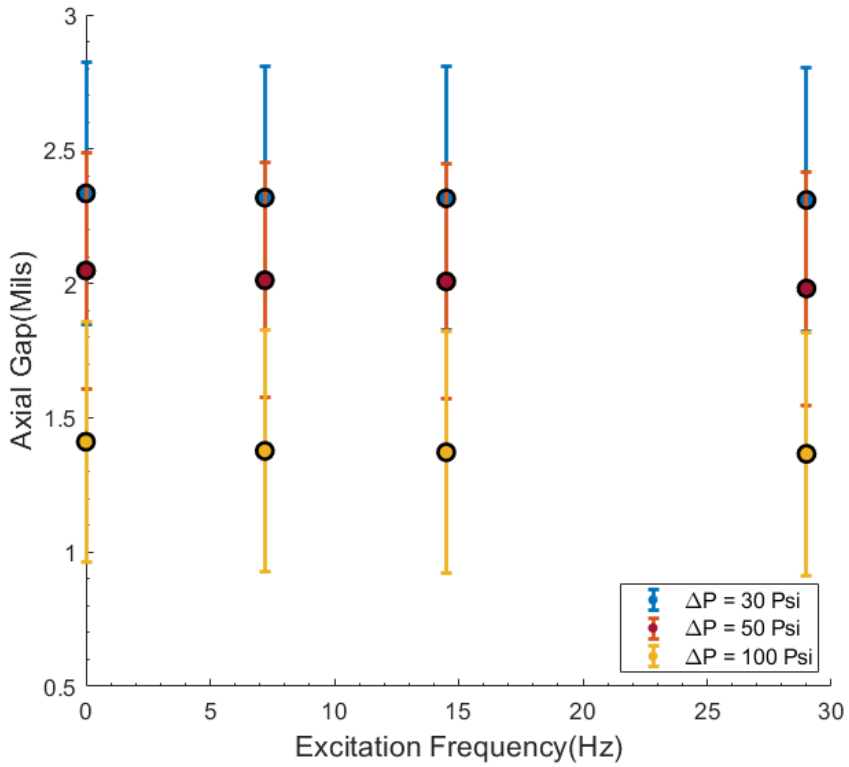

Figure 5.4: Average axial gap vs. excitation frequency

The trend continues for all of the levels of excitation shown during testing. The experimental trends from these tests differ from those reported in Figure 4.3 due to the different geometry of the seal and the corresponding pressure compensation design configuration. The mechanical seal used in this testing has a larger ratio of its effective area available for the closing force of the outer pressure to the effective area available for the opening force created by the inner pressure. Meaning that the geometry of the seal was designed for operating in the higher end of the pressure range.

While the film thickness decreasing with an increase in pressure is one major takeaway from Figure 5.4, another trend that may be of note is the film thickness relationship to the excitation frequency. All three chamber pressures seem to show a slight decline in film thickness as the

excitation frequency increases. A view of this trend on the magnitude of the actual film thickness will give more insight into its importance. The film thickness can be estimated by using Equation 4.1 with the leakage rate from the baseline trial. The difference in the calculated film thickness and the axial gap of the baseline trial can be subtracted from all of the axial gap readings at the different excitations. While this difference is a very rough estimate of what the actual difference would be, this does provide a reasonable scale to observe how the film thickness behaves with external vibration. The results of this exercise for the 30 Psi test case can be seen in Figure 5.5. Uncertainty of the data points Figures 5.5, 5.6, and 5.7 are the same as their corresponding values in Figure 5.4.

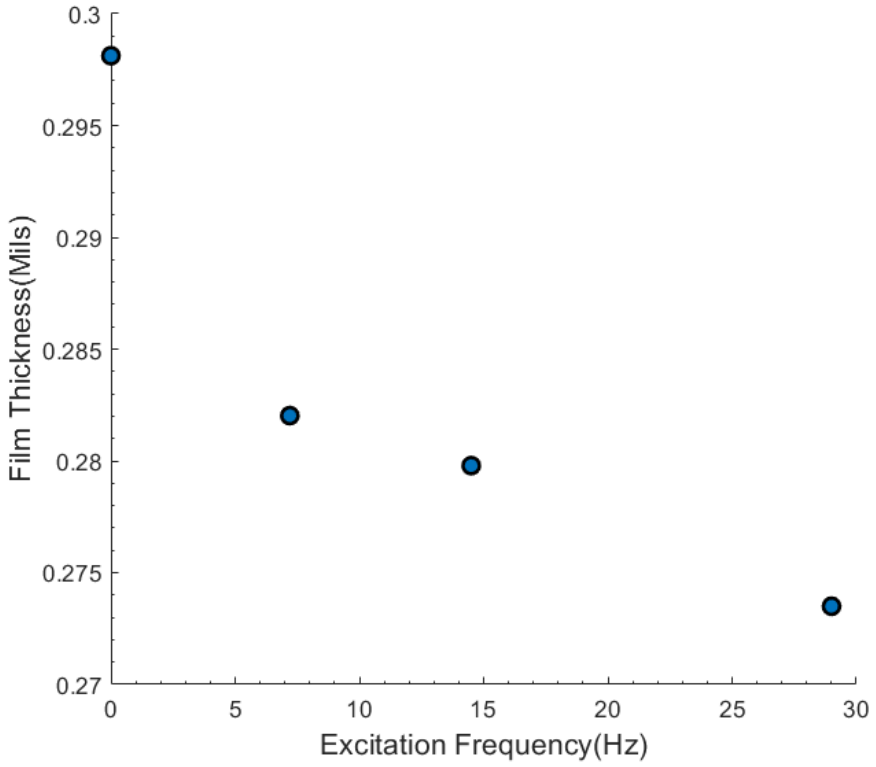

Figure 5.5: Estimated film thickness at 30 psi vs. excitation frequency

Observing the film thickness in this fashion shows that there is a downward trend with an increase in excitation frequency. The largest drop being when the excitation is first introduced to the system. Applying this method of calculating the film thickness to the other pressure trials provides us Figures 5.6 and 5.7.

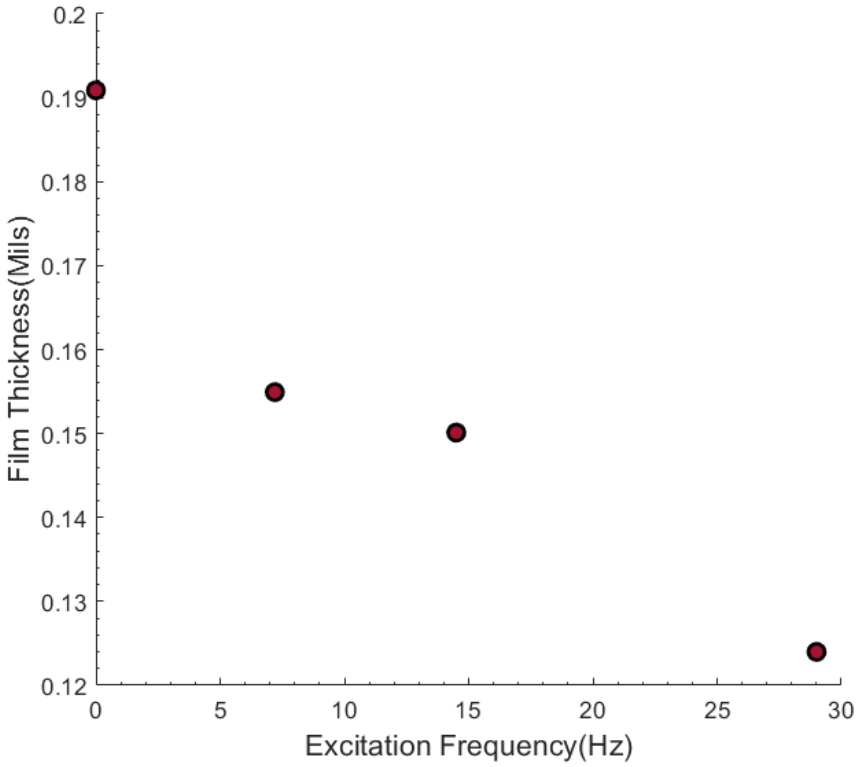

Figure 5.6: Estimated film thickness at 50 psi vs. excitation frequency

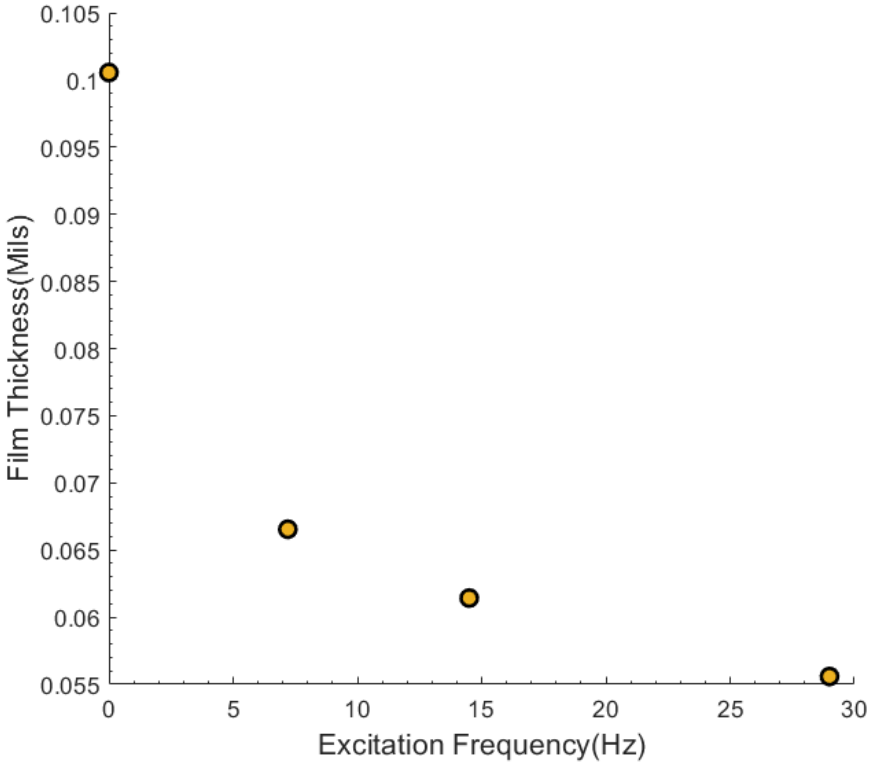

Figure 5.7: Estimated film thickness at 100 psi vs. excitation frequency

These estimated film thicknesses are within the same magnitude as the assumed film thicknesses for the predictions made by Childs and Norrbin [18] when considering the pressure differential and the size of the seal. The drop in film thickness is small, especially for the 30 psi case(0.0025 mils), and with the biggest drop being for the 50 psi case(0.006 mils), however there does not seem to be a relationship between this drop and the pressure differential of the seal. The consistency of a decrease in average film thickness with an increase in excitation frequency across all of the data strongly suggests that the externally induced lateral/pitch vibrations have an effect on the film thickness of the mechanical seal. The impact of frequency on film thickness is further illustrated when the axial vibration response is plotted within the frequency domain. The vibration response for 30, 50, and 100 psi in the frequency domain can be seen in Figures 5.8a, 5.8b, and 5.8c respectively.

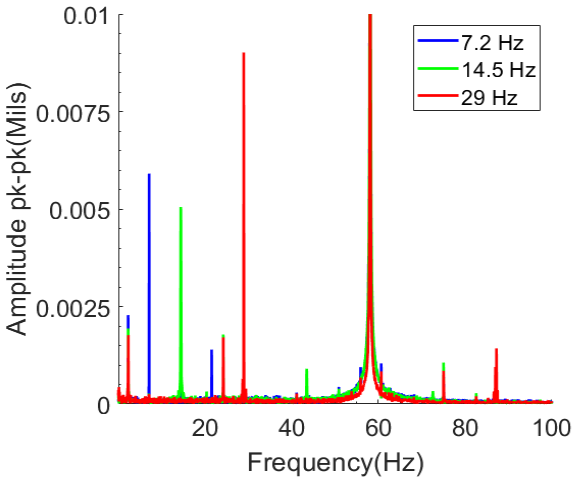

(a) Axial vibration response vs. frequency at 30 psi

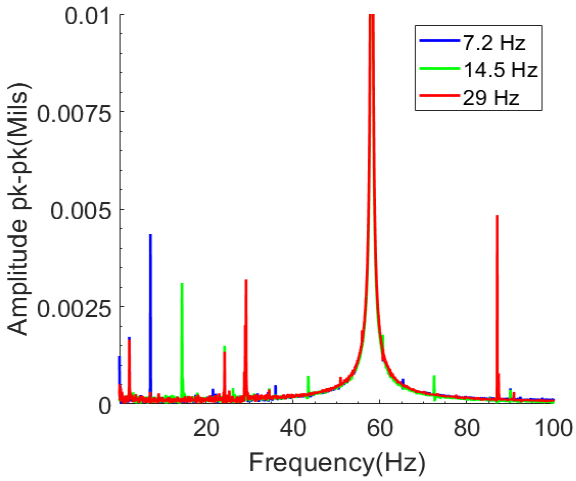

(b) Axial vibration response vs. frequency at 50 psi

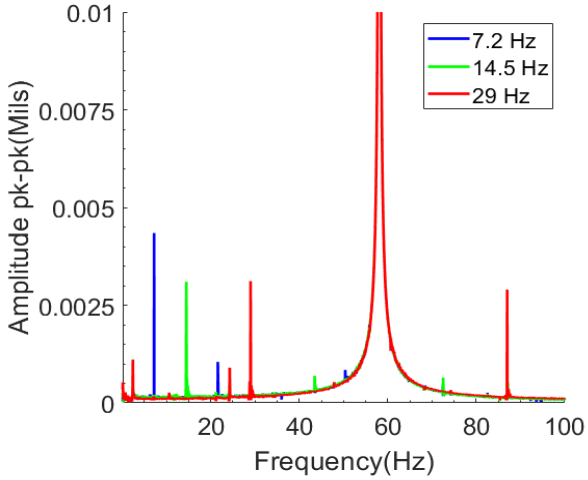

(c) Axial vibration response vs. frequency at 100 psi

Figure 5.8: axial vibration response vs. frequency

The scale of the y-axis was limited to adequately show frequencies besides the motor's running speed. At 58.3 Hz the amplitude is between 0.2 and 0.35 depending on the trial. This indicates that the motor vibration dominates over the external lateral vibrations as its amplitude is two orders of magnitude higher than that of the excitation frequencies. The excitation frequencies still show an impact in the frequency domain as their amplitudes are distinguishable from the spectral noise. Each excitation frequency also shows a 2x, 3x, 4x, and so on(multiples of 2 do not show up as the excitation frequencies are 2x of the previous trial's excitation frequencies), however the 3x seems

to be the most prominent with the 29 Hz being exceeded in the 50 psi set by its 3x counterpart. It is worth noting that the 29 Hz 2x and 14.5 Hz 4x could not be observed as that is the motor frequency. Whether this supersynchronous excitation is linked to the seal or the overall system will be observed in a later section when the rotor response is reviewed. While smaller in magnitude, there are two additional frequencies that do not seem to relate at all to excitation of the system. These frequencies, 2.4 Hz and 24.3 Hz are present in the baseline trials, which can be seen in Figure 5.9.

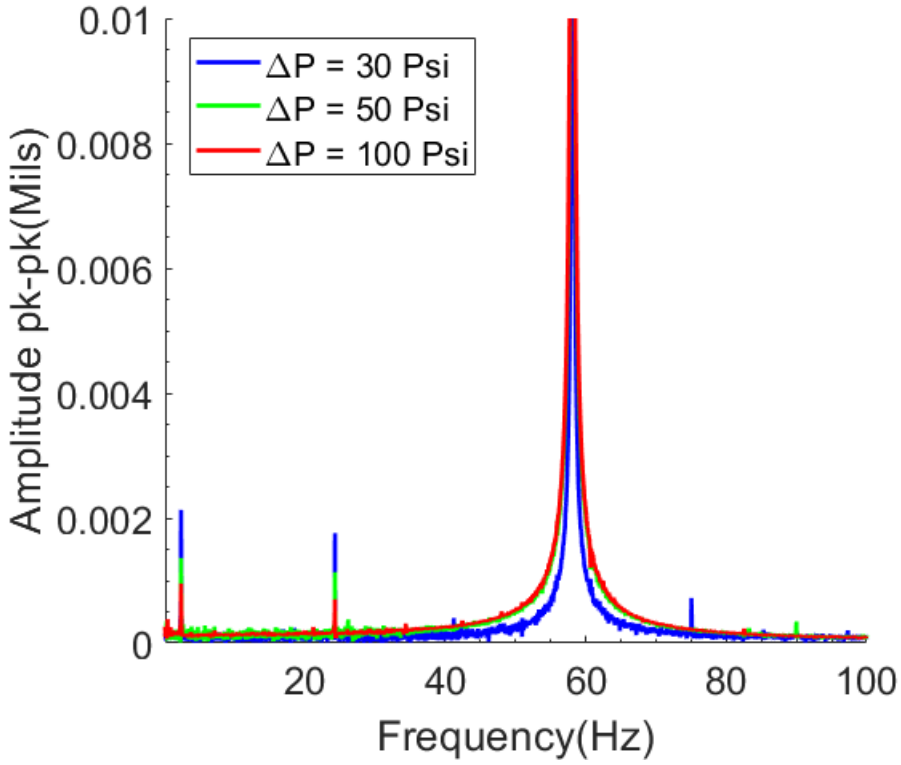

Figure 5.9: Axial vibration response with no external excitation vs. frequency

It is clear that these are vibrations excited by the rotor, however it is still possible that the external vibrations have an impact. From Figure 5.9 it seems that there is a pressure dependence on these vibrations as the amplitude is lower at higher chamber pressures, which suggests that these vibrations are related to the test chamber. The presence of these frequencies in other parts of the

system will help answer this question and will be explored in a later section.

While it is evident from the data that the externally induced lateral/pitch vibrations have an impact on the film thickness of the mechanical seal, the question remains as to whether this impact is significant. While observing the average film thickness is a good method for providing a simplified view of the seal performance, this does not provide the whole picture. The film thickness is not a constant value during operation, as shown by the frequency components, it is frequency dependent and oscillates during operation. Figures 5.10a, 5.10b, and 5.10c show how the film behaves during 0.1 second time frame.

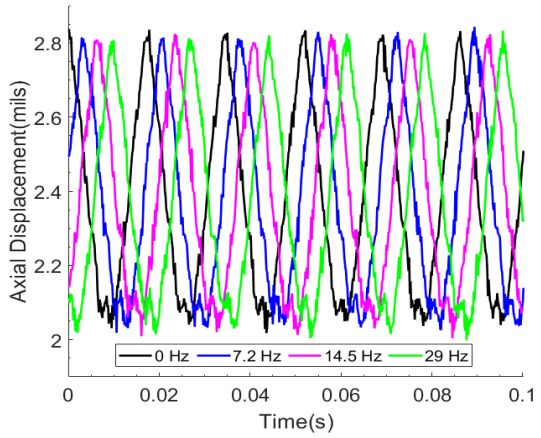

(a) Axial vibration at 30 psi

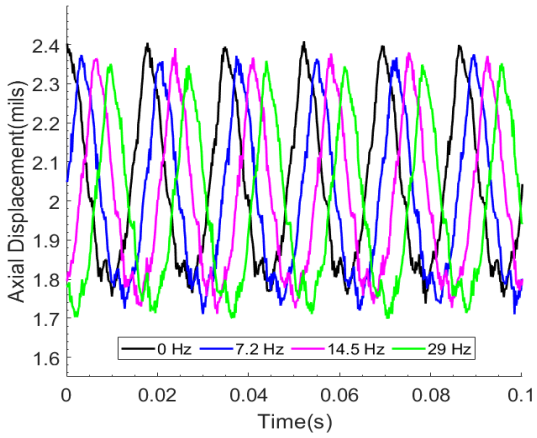

(b) Axial vibration at 50 psi

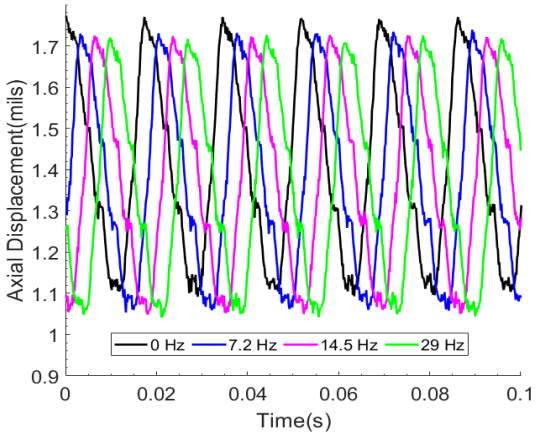

(c) Axial vibration at 100 psi

Figure 5.10: Axial vibration response vs. time over 0.1 seconds

The phase of these responses in reference to each other is irrelevant, the phase was set for the plot to make the individual curves distinguishable from each other. The trend of film thickness decreasing with frequency is still prevalent in this response, as the peaks of the vibration response curves can be seen decreasing with the increase in excitation frequency. However, what these figures demonstrate is that while the average film is decreasing with an increase in excitation frequency, the amplitude of the vibration response remains unchanged and is far larger than the difference in the peaks of the vibration. This means that while there is an influence of the excitation on the axial response, it is negligible during the span of operation. This is further supported by frequency domain results showing the magnitudes of the peaks for the excitation frequencies were insignificant to the magnitude of the motor's vibration response.

The film thickness has been shown to be frequency dependent. This disagrees with the assumption of the model discussed in Section 4.2 that film thickness is independent of frequency. An increase in the frequency of excitation shows a decrease in the average film thickness. However, this decrease is seen to be insignificant as the scale at which this decrease occurs is minor when compared to the amplitude of vibration seen in the axial direction. Furthermore, the lack of frequency dependence seen in the leakage of the mechanical seal supports this as film thickness has a cubic relationship with leakage and so a change that could be considered noteworthy would have shown a decrease in leakage. In regards to the film thickness, the external lateral vibrations have a negligible impact the performance of the flexibly mounted rotor mechanical seal, while leakage has no apparent effect.

5.2 Seal and Rotor Response

Vibration response of the rotor during operation was recorded at both the drive end(DE) and non-drive end(NDE) of the rotor. The response was recorded parallel to the stingers of the shakers, with an xy coordinate system being used. Facing the seal from the NDE of the rig, the coordinate system can be visualized with Figure 5.11.

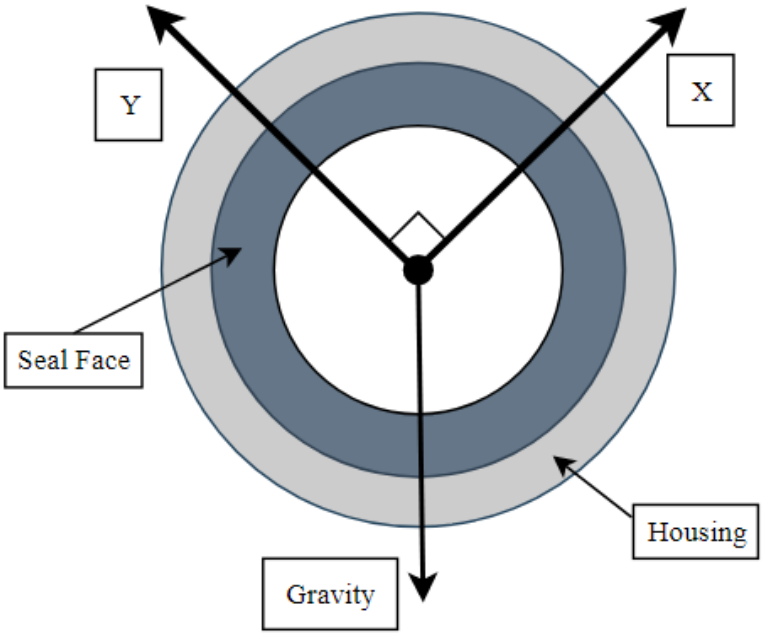

Figure 5.11: Rotor cartesian coordinate system

To fully appreciate the impact the shakers have on the system, the dynamic load they applied needs to be observed. Figure 5.12 shows one of the shakers applied loads at the three excitation frequencies during the 30 psi set of trials.

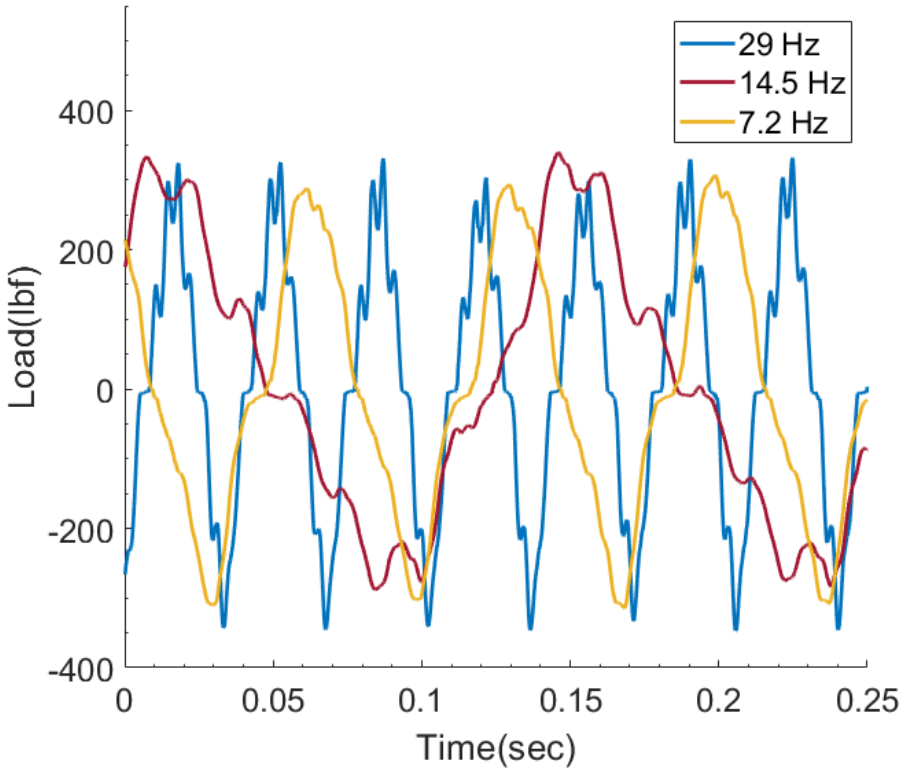

Figure 5.12: Shaker load vs. time

From this data it is clear, that while the frequency of the load applied between excitation increases, the amplitude of this load remains constant throughout testing.

The NDE data also includes direct measurements of the rotating portion of the seal's lateral vibrations, while the DE data is measurements of the rotor on the opposite side of the shaker from the mechanical seal. The response of the rotor is zeroed based on the baseline measurements for each set of trials. Figures 5.13 show the DE response of the rotor at 30, 50, and 100 psi over a four second interval.

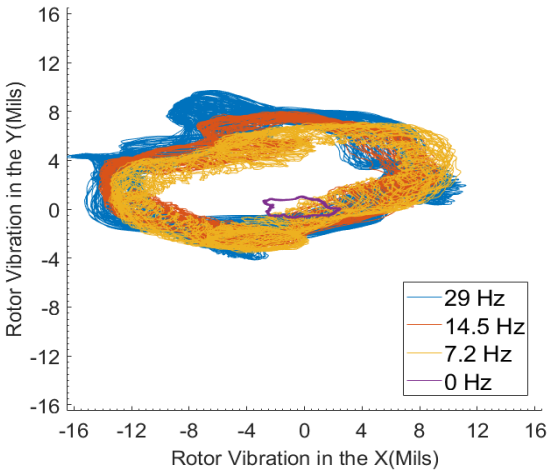

(a) DE rotor vibration response at 30 psi

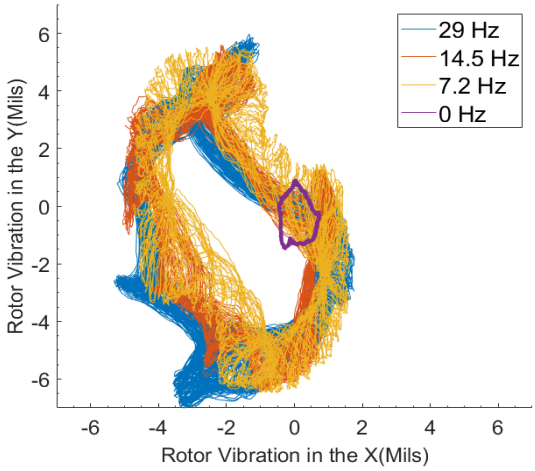

(b) DE rotor vibration response at 50 psi

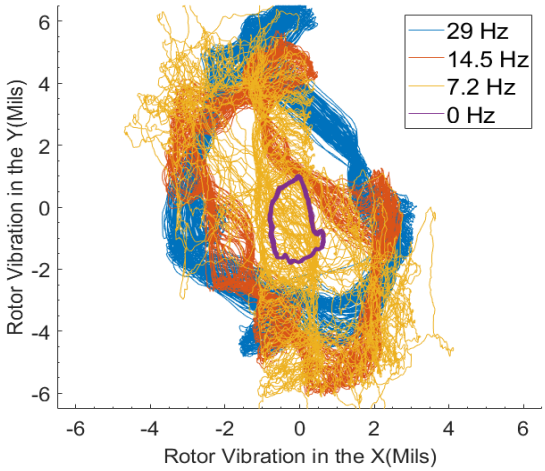

(c) DE rotor vibration response at 100 psi

Figure 5.13: DE rotor vibration response

The first finding from these plots worth noting is how the responses with forced excitation are not centered with the baseline trial for the 30 and 50 psi trials. The data suggests that the rotor center moves once excitation is exerted upon the system. This is further supported by the fact that the 100 psi set of trials was ran directly after the 50 psi set, implying that the rotor center "settles" after first experiencing excitation. Aside from the aforementioned baselines, the different excitation levels keep a consistent zero with each other, with visually little variation in the shape of the vibration and changes in amplitude that are less than 10%. The NDE response is of greater interest as this is measuring the actual lateral vibration of the seal. The NDE vibration response at 30, 50, and 100 psi over a four second interval can be seen in Figure 5.14.

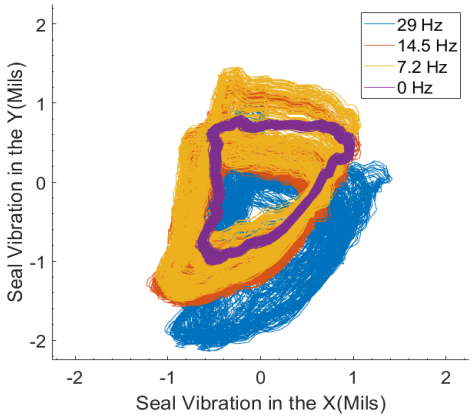

(a) NDE rotor vibration response at 30 psi

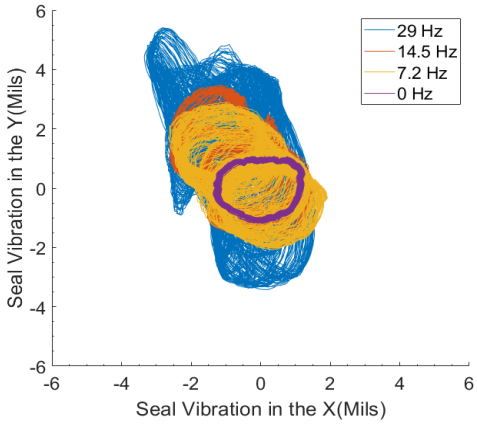

(b) NDE rotor vibration response at 50 psi

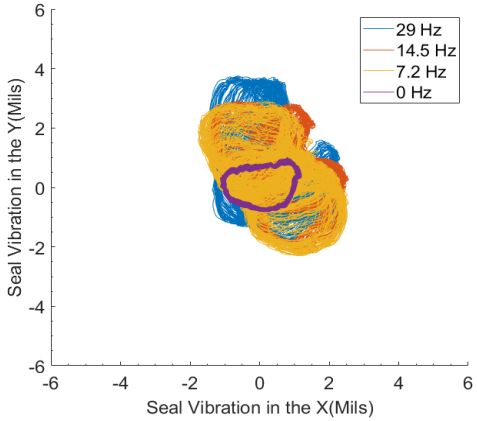

(c) NDE rotor vibration response at 100 psi

Figure 5.14: NDE rotor vibration response

The change in the rotor equilibrium position seen in the DE is not as visually prevalent in the NDE plots, however this could be due to the NDE having a significantly smaller amplitude of vibration across all of the trials. The NDE has a smaller amplitude of vibration due to the DE being where the actual excitation is induced, whereas the NDE is on the opposite side of the rotor. While there does not seem to be any trend with the response with respect to the pressure, the figures suggest that there is a greater amplitude of vibration at higher levels of excitation. Filtering the data by recon-structuring the time signal using the Fourier components associated with the excitation frequencies a fit of provides a clearer view of the impact frequency has on the rotor and seal response. Figures 5.15, 5.16, and 5.17 show the NDE rotor response filtered while Figures 5.18, 5.19, and 5.20 show the DE rotor response filtered. The orbits are centered in the same manner about their respective baselines from Figures 5.13 and 5.14. These orbits show the response over an eight second interval.

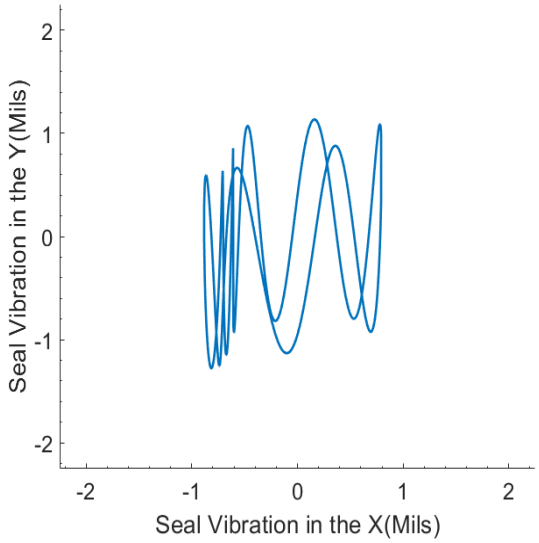

(a) NDE rotor fitlered vibration response at 30 psi and 7.2 Hz

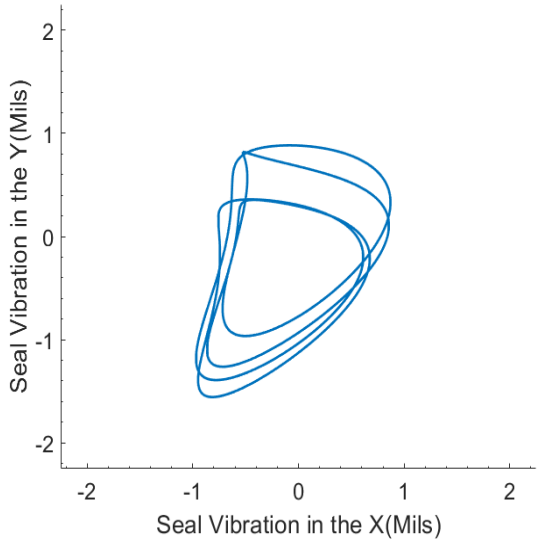

(b) NDE rotor fitlered vibration response at 30 psi and 14.5 Hz

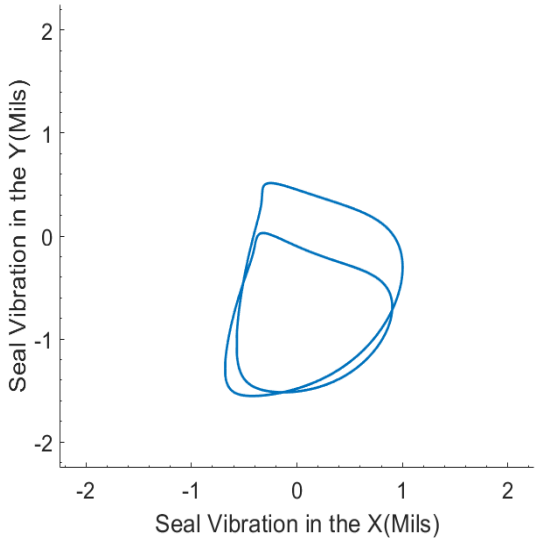

(c) NDE rotor fitlered vibration response at 30 psi and 29 Hz

Figure 5.15: NDE rotor fitlered vibration response at 30 psi

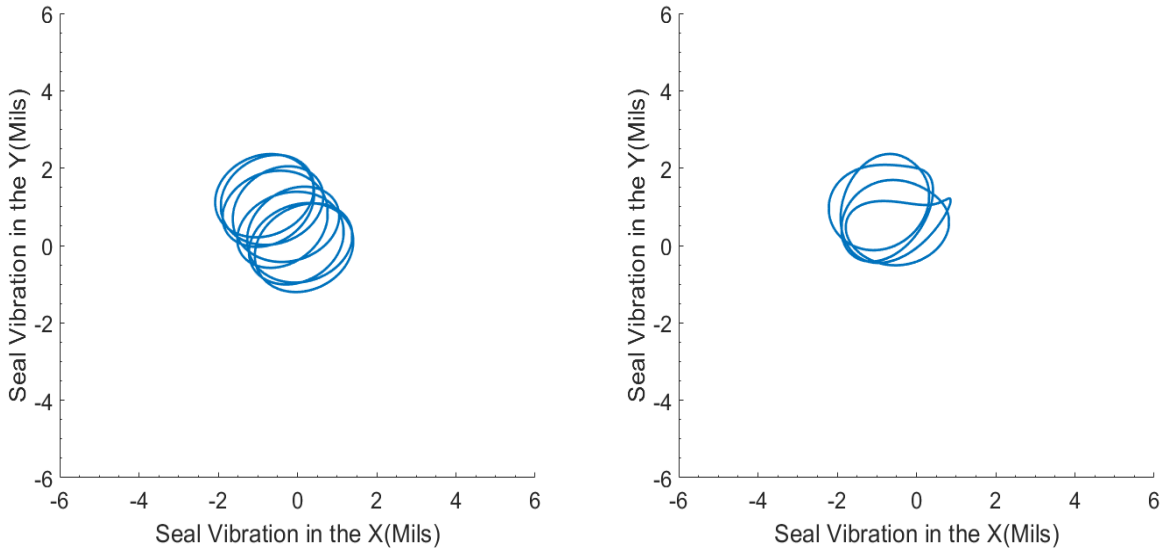

(a) NDE rotor fitlered vibration response at 50 psi and 7.2 Hz

(b) NDE rotor fitlered vibration response at 50 psi and 14.5 Hz

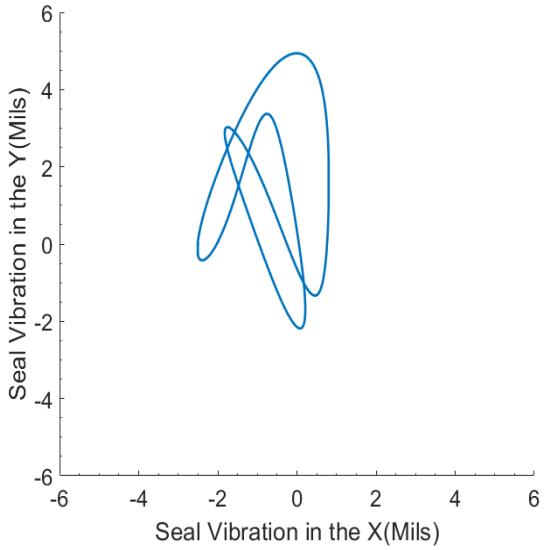

(c) NDE rotor fitlered vibration response at 50 psi and 29 Hz

Figure 5.16: NDE rotor fitlered vibration response at 50 psi

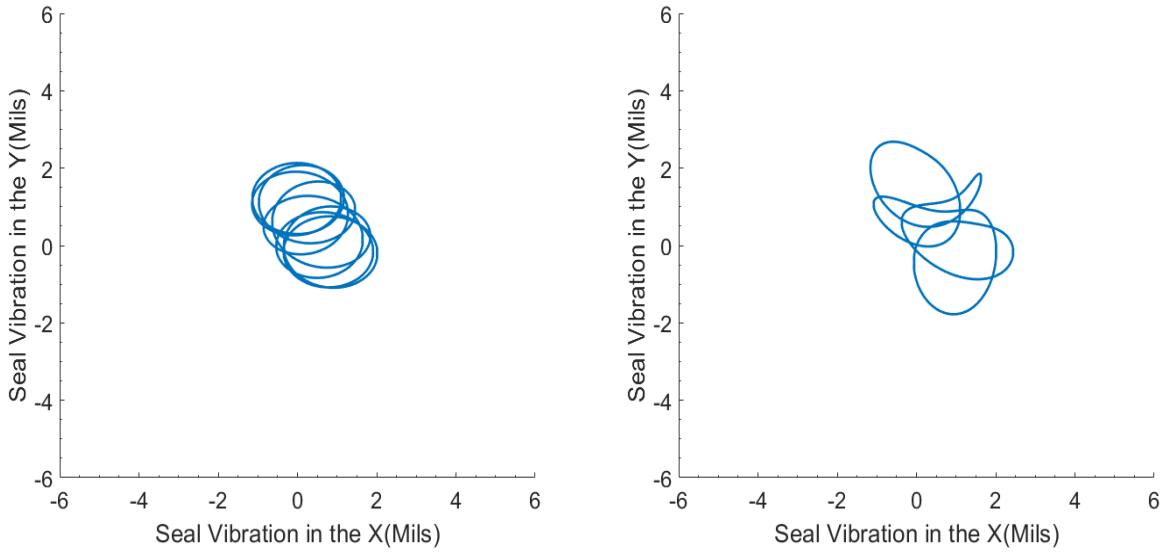

(a) NDE rotor fitlered vibration response at 100 psi and 7.2 Hz

(b) NDE rotor fitlered vibration response at 100 psi and 14.5 Hz

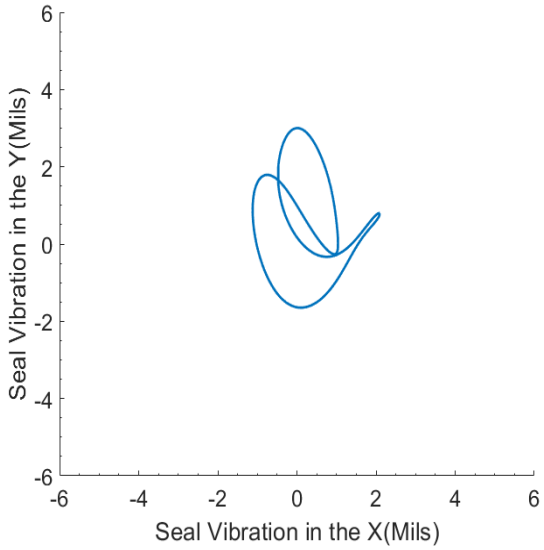

(c) NDE rotor fitlered vibration response at 100 psi and 29 Hz

Figure 5.17: NDE rotor fitlered vibration response at 100 psi

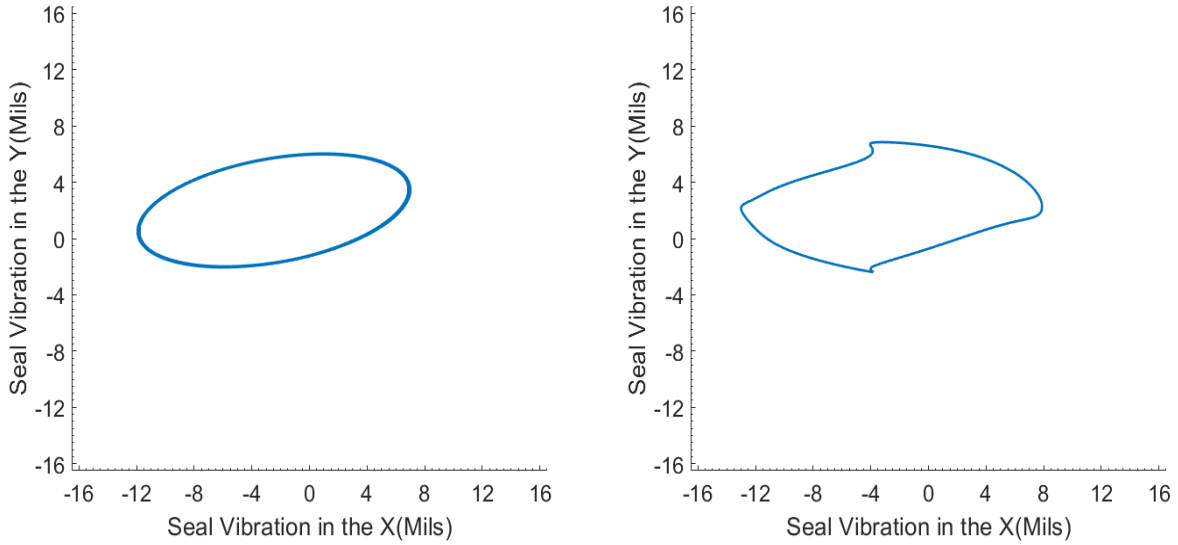

(a) DE rotor fitlered vibration response at 30 psi and 7.2 Hz

(b) DE rotor fitlered vibration response at 30 psi and 14.5 Hz

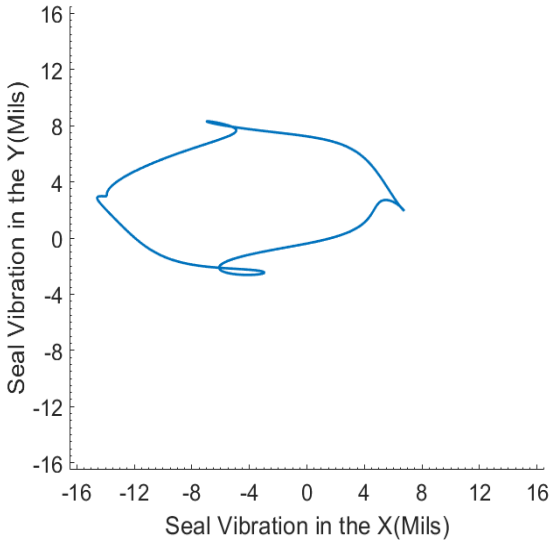

(c) DE rotor fitlered vibration response at 30 psi and 29 Hz

Figure 5.18: DE rotor fitlered vibration response at 30 psi

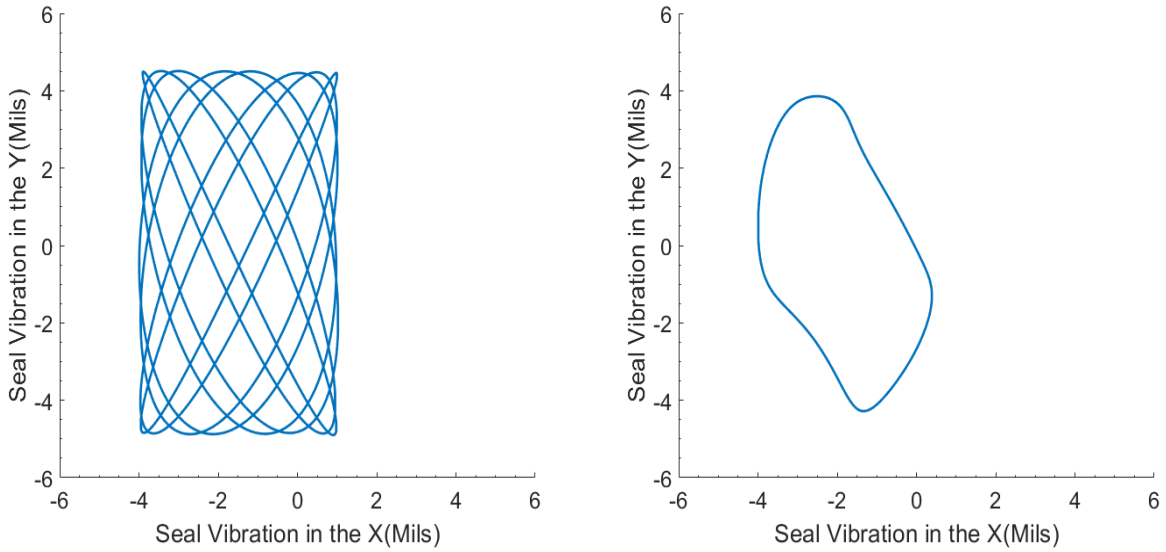

(a) DE rotor fitlered vibration response at 50 psi and 7.2 Hz

(b) DE rotor fitlered vibration response at 50 psi and 14.5 Hz

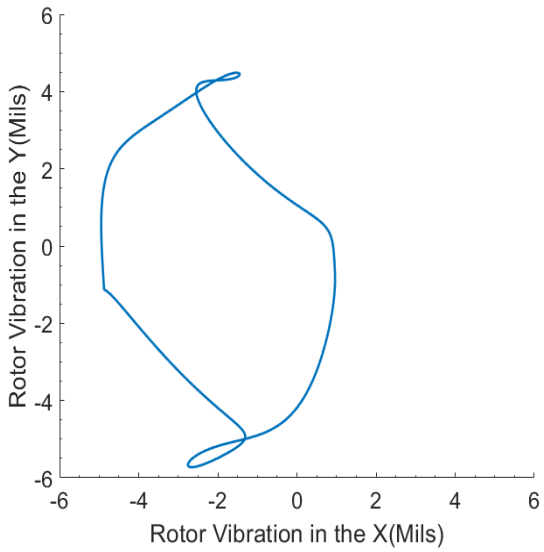

(c) DE rotor fitlered vibration response at 50 psi and 29 Hz

Figure 5.19: DE rotor fitlered vibration response at 50 Psi

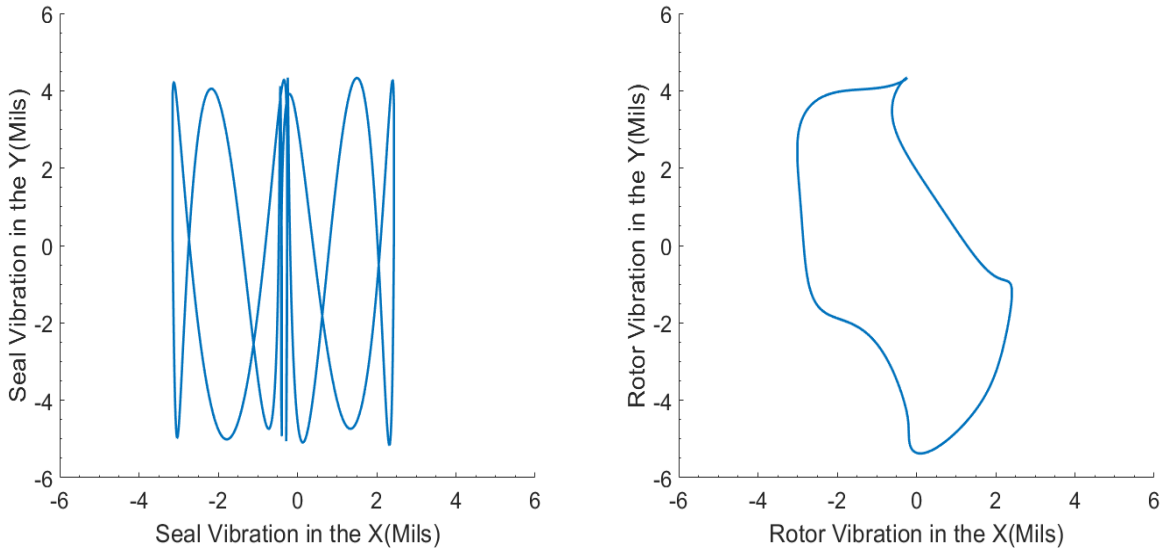

(a) DE rotor fitlered vibration response at 100 psi and 7.2 Hz

(b) DE rotor fitlered vibration response at 100 psi and 14.5 Hz

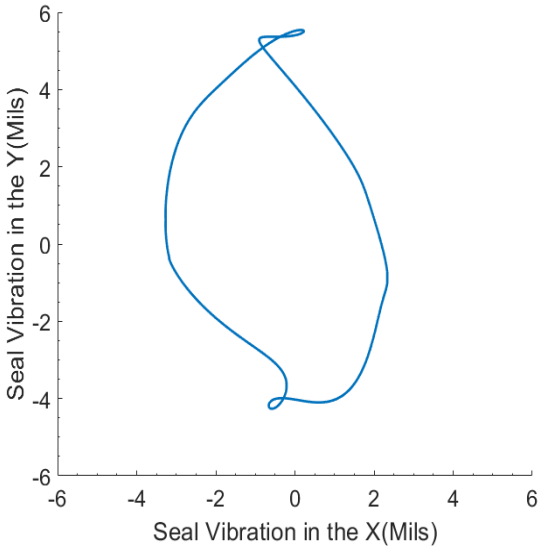

(c) DE rotor fitlered vibration response at 100 psi and 29 Hz

Figure 5.20: DE rotor fitlered vibration response at 30 psi

The first observation that can be made from the filtered orbits is that the amplitude of vibration does not change by a noticeable amount with excitation. These orbits are actually smaller by up to 25% than their unfiltered counterparts seen in the previous figures. What's most interesting is

that the seal, NDE rotor, seems to have a less erratic pattern of motion at higher frequencies as the higher frequency orbitals show less paths of motion. The rotor, DE rotor, follows this trend except for the 30 psi of data.

Looking at the average amplitudes experienced at each frequency provides a simpler view of the data to evaluate frequency dependence. Figures 5.21 and 5.22 show the average NDE and DE vibration amplitudes respectively versus the excitation frequency.

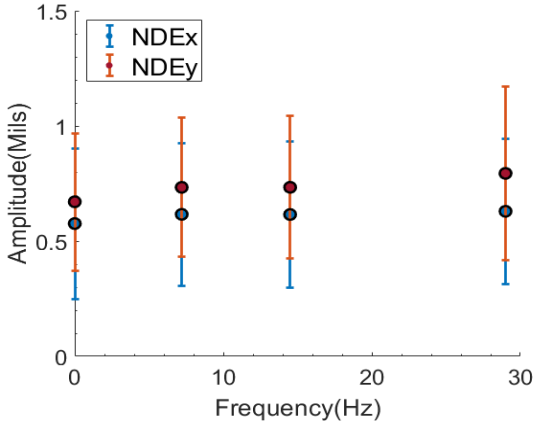

(a) NDE average vibration amplitude at 30 psi

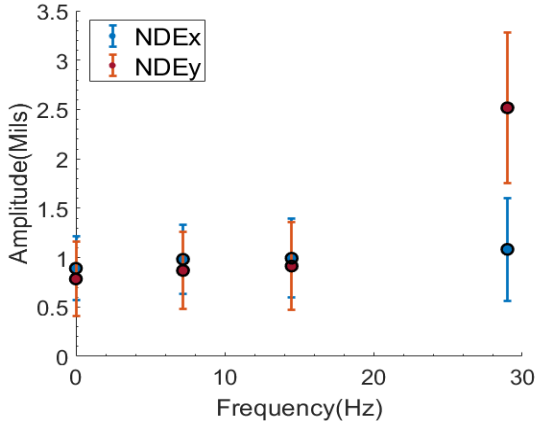

(b) NDE average vibration amplitude at 50 psi

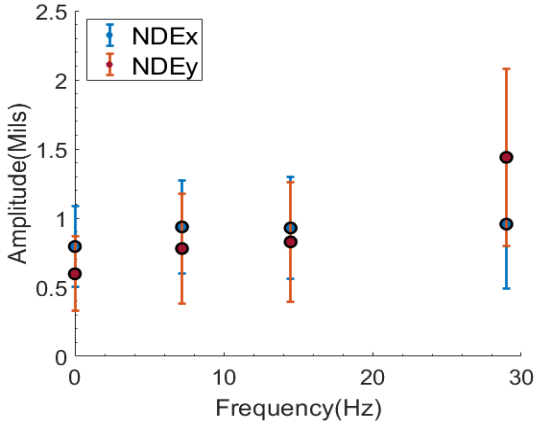

(c) NDE average vibration amplitude at 100 psi

Figure 5.21: NDE average vibration amplitudes

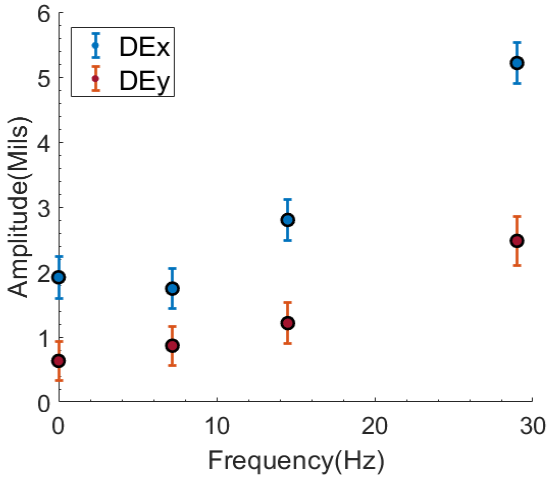

(a) DE average vibration amplitude at 30 psi

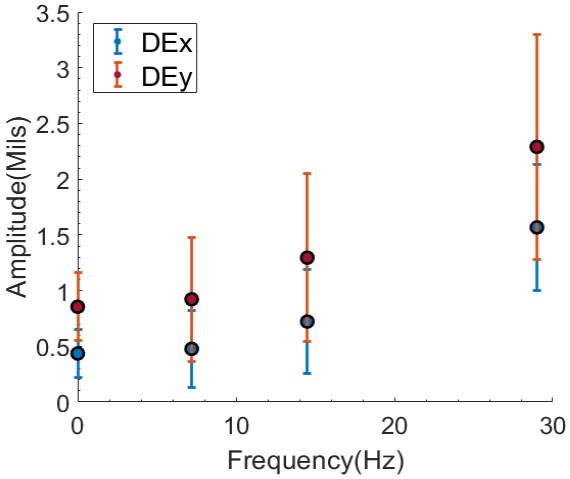

(b) DE average vibration amplitude at 50 psi

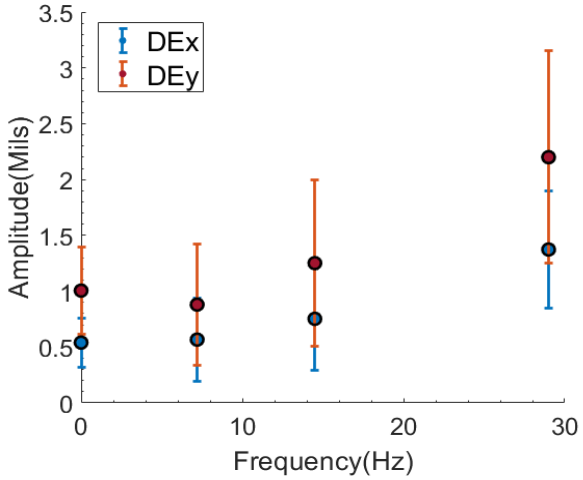

(c) DE average vibration amplitude at 100 psi

Figure 5.22: DE average vibration amplitudes

The DE vibration amplitudes seen in Figure 5.22 shows a clear increase with excitation frequency across all of the trials, with the 29 Hz trial being two to three times as high as its baseline counterpart depending on the trial. The NDE amplitude seen in Figure 5.21 shows an increase in amplitude once excitation is added to the system, however the amplitude does not exhibit a consistent behavior between trials with an increasing excitation frequency, with a relatively large increase in amplitude being seen at 29 Hz, but only for the measurements in the Y axis. These results for average amplitude can be used to quantify the response of the seal via its lateral transmissibility.

Using Equation 4.2 with the NDE average amplitude as A_s and the DE average amplitude as A_r yields the results shown in Figure 5.23.

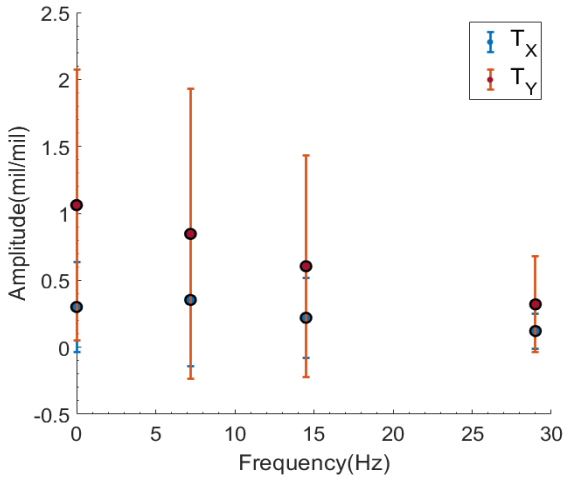

(a) Lateral transmissibility at 30 psi

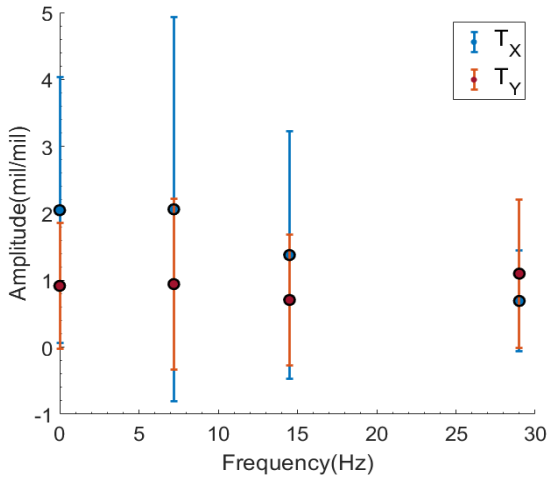

(b) Lateral transmissibility at 50 psi

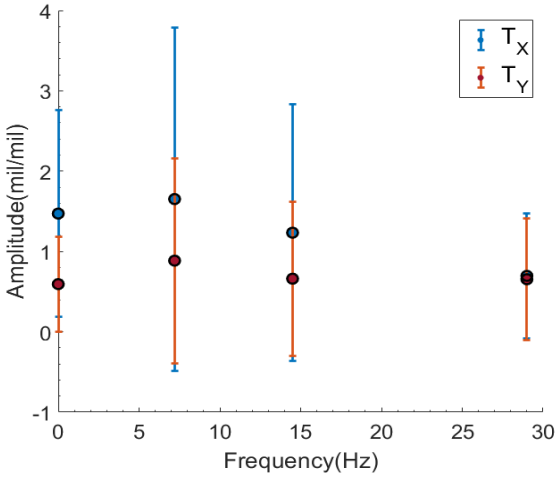

(c) Lateral transmissibility at 100 psi

Figure 5.23: Lateral transmissibility

From these results, there is not a conclusive trend on how the transmissibility behaves when excitation is added to the system, however the majority of the results suggest that there is a decrease in the seal response at higher excitation frequencies. The frequency dependence of the seal

vibration can be further explored via a Fourier transform of the NDE Vibration response. Figure 5.24 shows the vibration response versus frequency for the baseline trials.

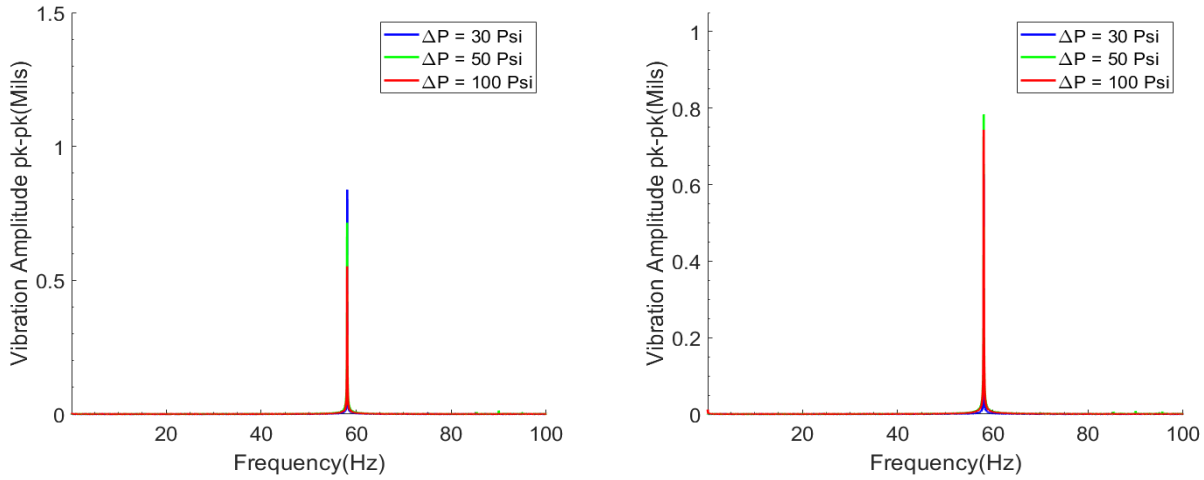

(a) NDE_y baseline vibration response

(b) NDE_x baseline vibration response

Figure 5.24: NDE baseline vibration response in the frequency domain

As one would expect the motor has a prominent impact on the lateral vibration experienced by the seal, with the only major peak coinciding with the motor's operating frequency. It is important to note the magnitude of this peak as the excitation frequencies will likely impact the vibration at the running speed's frequency. The 24.3 Hz peak seen in the axial vibration data did appear within the NDE data with a nearly identical magnitude, indicating that this vibration is associated with the system. However, the incredibly small magnitude of this vibration(0.003 mils) means this is negligible. The NDE vibration response with an external excitation versus frequency can be seen in Figures 5.25 and 5.26.

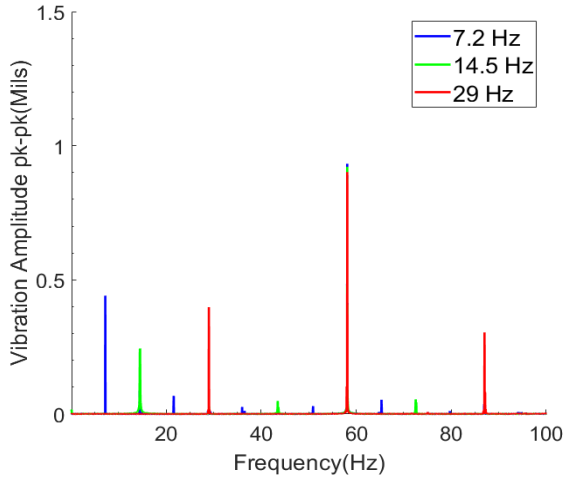

(a) NDE_y vibration response at 30 psi

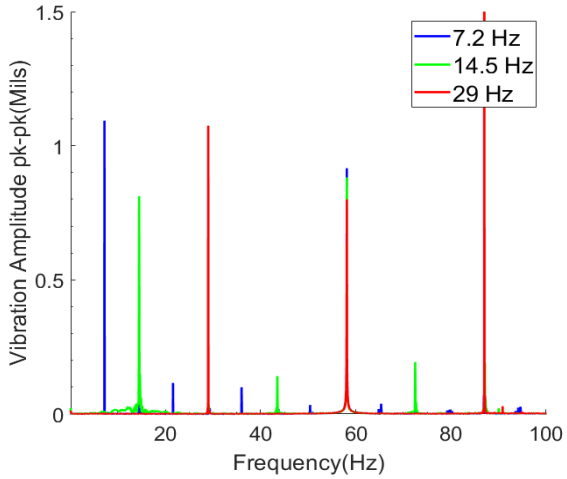

(b) NDE_y vibration response at 50 psi

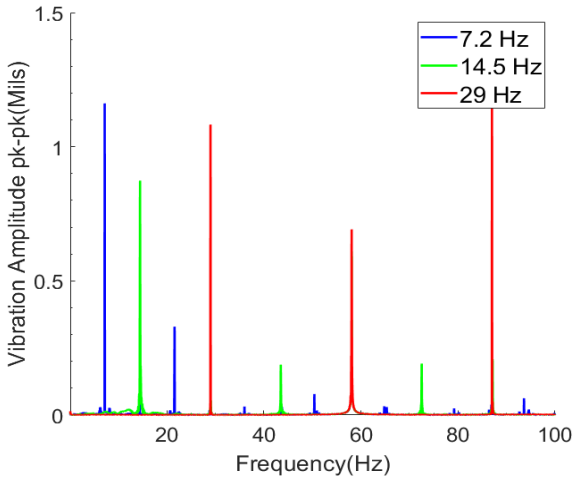

(c) NDE_y vibration response at 100 psi

Figure 5.25: NDE_y vibration response in the frequency domain

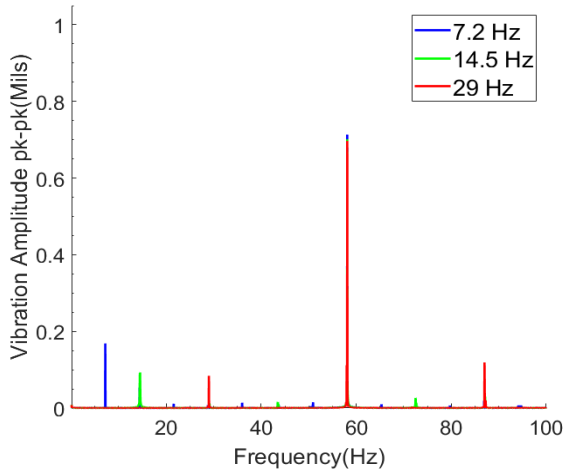

(a) NDE_x vibration response at 30 psi

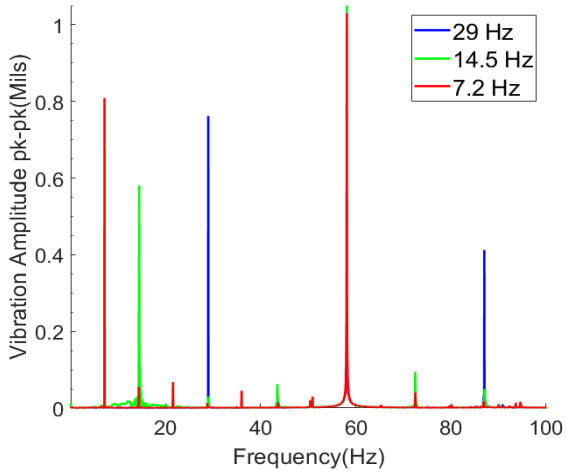

(b) NDE_x vibration response at 50 psi

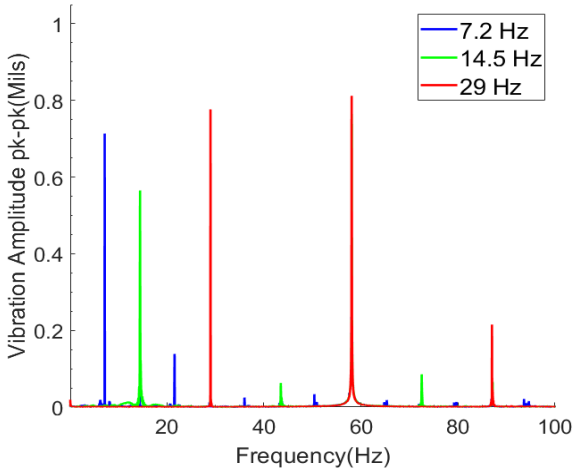

(c) NDE_x vibration response at 100 psi

Figure 5.26: NDE_x vibration response in the frequency domain

Figure 5.25b was cut off in the y axis at an amplitude of 1.5 for the purpose of comparing with Figures 5.25a and 5.25c at the same scale, however the response at 87 Hz, 3x of the 29 Hz excitation, actually reached an amplitude of 2.5 mils. Each frequency for each trial shows a vibration response that is within the same magnitude of the amplitudes of vibrations shown in Figure 5.21. Furthermore, all of the frequency responses show an increase in the peak corresponding with 58.3 Hz, meaning the excitation added to that vibration response with 8x, 4x, and 2x vibrations for 7.2 Hz, 14.5 Hz, and 29 Hz respectively. These findings indicate that there is indeed a frequency

dependence on the lateral vibration for the seal and that it has a significant impact on its response. The results seem to indicate there is not an an upward/downward trend in the magnitude of this response when related to frequency as the 14.5 Hz response is consistently seen to be the smallest of the 1x vibrations, with the exception of the results seen in Figure 5.26a.

The rotor response and seal response have both been shown to be influenced by the external lateral vibrations. The rotor vibration amplitude consistently increases with an increase in excitation frequency, while the seal vibration amplitude does not conclusively show this trend. Lateral transmissibility is shown to be inversely proportional to excitation frequency in most instances, however the 29 Hz excitation increases transmissibility in the y-direction for the 50 and 100 psi trials. The magnitude of the measured transmissibility of the seal coincides with the predictions shown in Figure 4.4. However a lack of a clear trend in the performance of the seal coupled with the difference in the magnitude between the predictions and experiments prevents drawing a conclusion about the damping models.

5.3 Power Consumption

Power consumption is a common metric used to characterize the performance of mechanical seals since it can be easily obtained and it is directly related to surface friction and operation cost. Friction is a parameter that seal manufacturers and end users want to minimize in order to increase the service life of components.[2]. Power consumption can be related to friction through torque, as the power consumption of a seal is simply the product of its rotational speed, ω, and the torque due to friction, T_f, see Equation 5.1.

$$P = \omega \times T_f \tag{5.1}$$

The torque due to friction in this equation is the sum of the torque from the sliding at the interface of the two seals, T_s, and the torque due to fluid drag from rotation, T_d. T_d at lower operating speeds can typically be considered to be insignificant when compared to T_s[2], but due to the constant running speed of this experiment and the relatively constant viscosity that was shown to exist in Figure 5.2, the fluid drag can be assumed to have been constant throughout testing. This means the power consumption is directly related to T_s, which can be described as 5.2.

$$T_s = r_s P_{close} f A_{int} \tag{5.2}$$

Where r_s represents the sliding radius of the seal, P_{close} represents the closing pressure or the chamber pressure, f represents the coefficient of friction, and A_{int} represents the interface area between the seals[2]. r_s and A_{int} are geometric properties of the seal and thus constant, while P_{close} is directly related to the measured chamber pressure. Friction is actually expected to be relatively constant as well as friction is related to the viscosity when full film lubrication is occurring[2]. In summary, these relations state that the power consumption should linearly increase with the chamber pressure, a significant deviation from that trend will suggest that the externally excited lateral vibrations impact the power consumption. Power consumption of the seal can be calculated based upon the measured rotational torque of the seal and the measured running speed. Figure 5.27

shows the average power consumption for the baseline trials compared to the respective pressures.

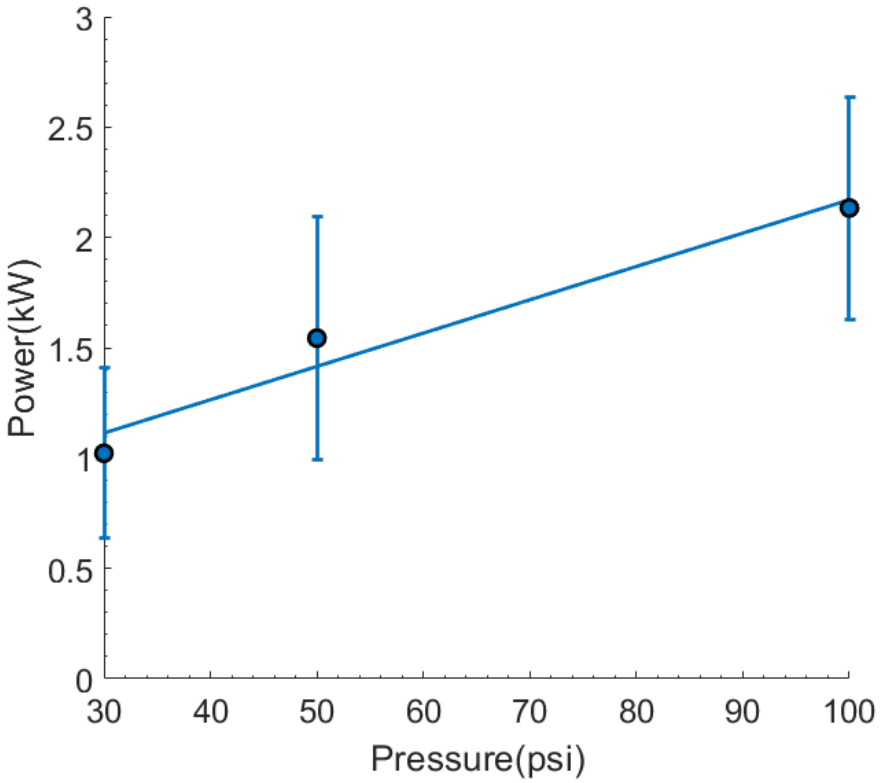

Figure 5.27: Baseline power consumption vs. chamber pressure

Figure 5.27 does not display a completely linear trend as would be expected, indicating that the friction did indeed change an appreciable amount between trials. Further applying Equation 5.1 to the excitation trials provides the results seen in Figure 5.28.

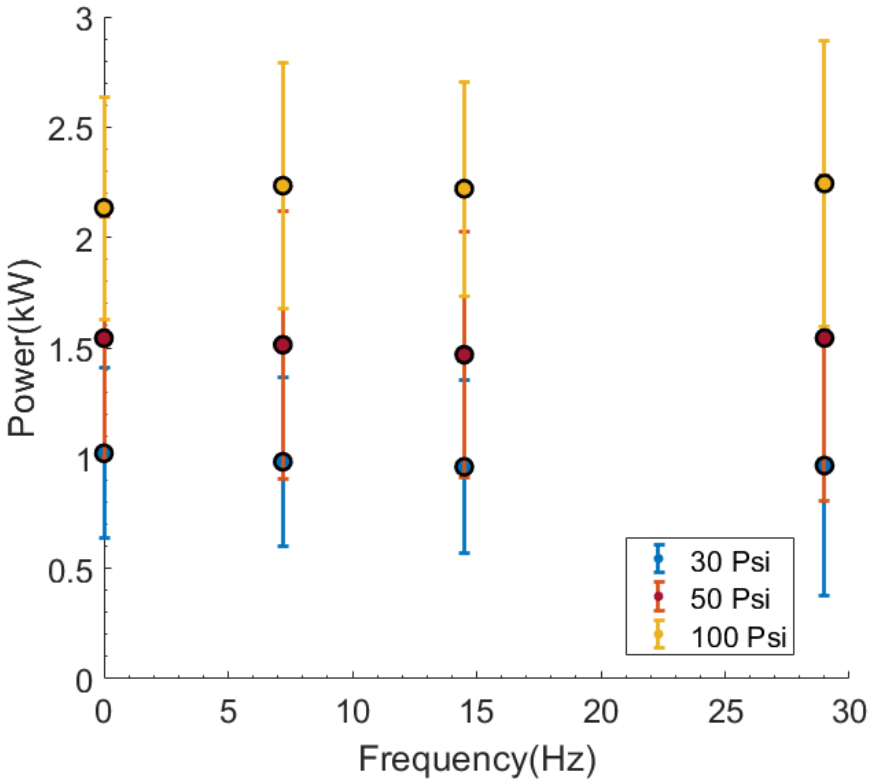

Figure 5.28: Power consumption vs. excitation frequency

These results mirror the leakage results from Figure 5.1 with no discernible relation to frequency and clear trend with respect to the pressure. A Fourier transform of the torque results for one pressure trial will confirm whether the power consumption is truly independent of frequency. Figure 5.29 displays the torque consumption of the seal versus frequency.

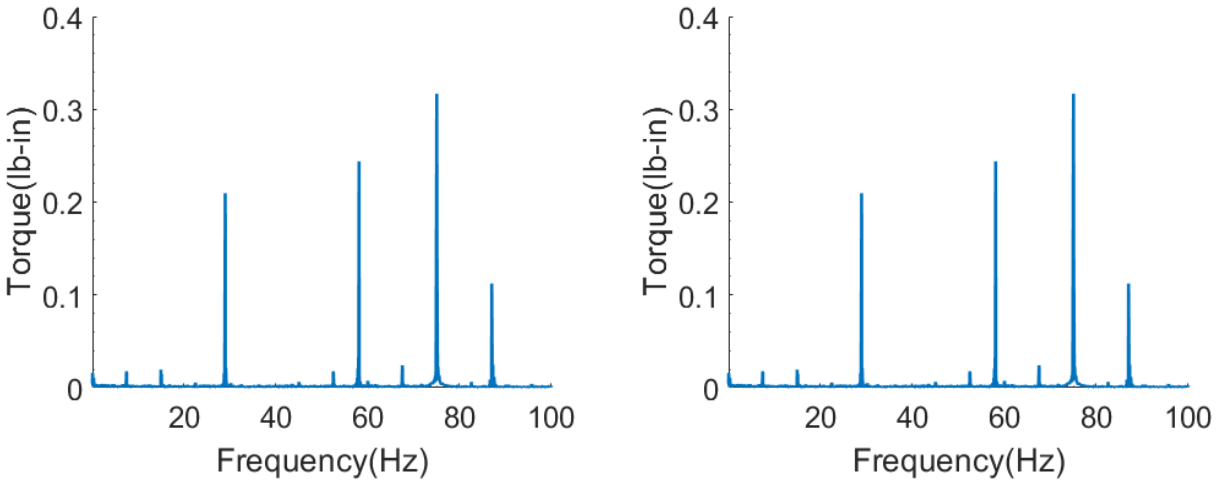

(a) Baseline torque response

(b) 7.2 Hz torque response

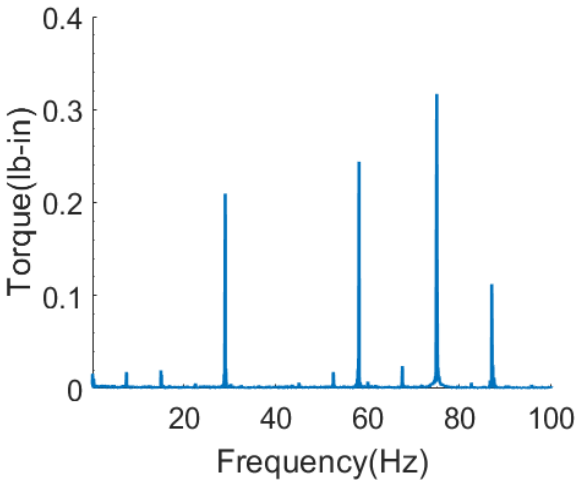

(c) 14.5 Hz torque response

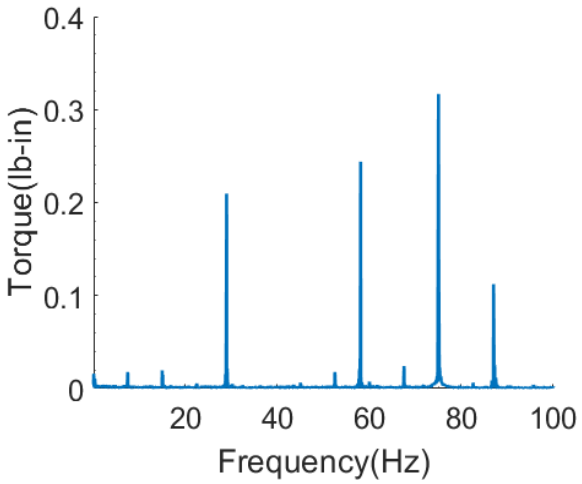

(d) 29 Hz torque response

Figure 5.29: Torque response in the frequency domain at 30 psi

While the torque does show dependence on the running speed, there is no apparent dependence of the torque on the excitation frequency. The power consumption of the mechanical seal is dependent upon the chamber pressure, but is independent of externally induced lateral/pitch vibrations

6. CONCLUSIONS

An FMR mechanical seal was tested in a test rig that mimics conditions of centrifugal pumps typically seen in industry. Subsynchronous lateral/pitched vibrations were externally exerted upon the rotor to create a conical mode of vibration. Relative radial and axial vibrations of the mechanical seal, torque, and leakage were continually monitored to evaluate the seal performance.

The leakage of the mechanical seal was found to be independent of the excitation frequency, but is negatively proportional to the chamber pressure magnitude. The inverse relationship between leakage and pressure contradicted previous results of testing done at Texas A&M, however this is due to the pressure compensation effect on the film thickness(i.e. larger closer force). Film thickness was found to decrease with an increase in the chamber pressure, which further supports this conclusion. The average film thickness decreased as the excitation frequency increased, indicating a frequency dependence. The axial vibration response seen in the frequency domain also shows this, meaning the film thickness of an FMR seal is influenced by external vibrations. However, the change in film thickness is an order of magnitude less than the amplitude of vibration of the film thickness. This along with the lack of a noticeable impact on the leakage of the mechanical seal means that frequency dependence of the film thickness is insignificant for subsynchronous excitations.

The lateral vibration amplitude of the rotor was found to have a notable frequency dependence through the analysis of its amplitude. This dependence shows an increase in vibration with an increase in excitation frequency. The lateral vibration of the rotating portion of the seal also shows a frequency dependence with its vibration amplitude and response within the frequency domain. However, this dependence does not follow a clear trend with the 29 Hz trial creating a comparably high amplitude for the 50 and 100 psi trials exclusively in the y-direction. It is unclear if this behavior is related to the system or is due to the imposed vibration. Nonetheless, all excitation trials showed a significant deviation from the baseline, so a frequency dependence is conclusive. Using the average lateral vibration amplitudes of the rotor and the seal, the lateral transmissibility

is found to have an overall downward trend. However, the aforementioned anomaly observed at the 29 Hz excitation trial, contradicts this trend and prevents any determination of the exact nature of the transmissibility's frequency dependence.

The power consumption of the seal was found to increase with chamber pressure, but at a rate that disagrees with theory. A possible explanation for this is an inconsistent coefficient of friction between trials caused by wearing of the seal face or a minor change in rig alignment between the 30 psi set of trials and the remaining trials. A change in viscosity could also impact this as friction for lubricated surfaces is directly proportional to viscosity. The trend of the temperature seen in Figure 5.2 does align with this hypothesis. Power consumption was found to be frequency independent as the average power consumption at constant pressures was not altered an appreciable amount by the variation of excitation frequency. Further analysis of the torque response for the 30 psi set of trials in the frequency domain supports this observation.

Further experimental work is needed to conclude whether the impact of the film thickness is significant as currently results suggest otherwise and determine the exact nature of the relationship between excitation frequency and transmissibilty. However, based on the frequency dependence of the film thickness and lateral transmissibilty, the results of the experiment work for this thesis indicate that external lateral/pitch vibrations have an impact on the performance of flexibly mounted rotor mechanical seals.

REFERENCES

[1] Shabbir, S., Uk, Garvey, S., and Dakka, S., 2019, "Aerospace Sealing Technology for Maintenance, Repair, and Overhaul of engines: a review," *24th Conference Of The International Society For Air Breathing Engines*.

[2] Mayer, E., 1981, "Mechanical Seals," *Butterworth-Heinemann*.

[3] Nau, B. S., 1997, "Mechanical seal face materials," *Proceedings of the Institution of Mechanical Engineers, Part J: Journal of Engineering Tribology*, Vol. 211, Paper No. 3, pp. 165–183.

[4] Lee, A. S. and Green, I., 1994, "Rotordynamics of a Mechanical Face Seal Riding on a Flexible Shaft," *Journal of Tribology*, Vol. 116, Paper No. 2, pp. 345–350.

[5] Minet, C., Brunetiere, N., Tournerie, B., and Fribourg, D., 2010, "Analysis and Modeling of the Topography of Mechanical Seal Faces," *Tribology Transactions*, Vol. 53, Paper No. 6, pp. 799–815.

[6] Merrill, J. B., 2009, "A Contemporary Guide to Mechanical Seal Leakage," *EagleBurgmann*.

[7] FSA Technical Committee, 2013, "How to Extend Mechanical Seal Life," *Pump & Systems*.

[8] Buck, G. S., 1992, "Mechanical Seal Reliability," *Centrifugal Pumps*, pp. 556–567, doi: 10.1016/B978-0-08-050085-0.50024-2.

[9] Stefanko, D. B. and Leishear, R. A., 2005, "Relationship Between Vibrations and Mechanical Seal Failures in Centrifugal Pumps," *Process Industries*, ASMEDC, pp. 5–12, doi:10.1115/IMECE2005-79176.

[10] Dietzel, W. and Vasko, J., "The Evolution and Application of Mechanical Seal Face Materials," *Texas A&M Turbomachinery Laboratory*.

[11] Denny, D., 1961, "Some measurements of fluid pressures between plane parallel thrust surfaces with special reference to radial-face seals," *Wear*, Vol. 4, Paper No. 1, pp. 64–83.

[12] Etsion, L., 1982, "A Review of Mechanical Face Seal Dynamics," *The Shock and Vibration Digest*, Vol. 14, Paper No. 3, pp. 9–14.

[13] Metcalfe, R., 1982, "Dynamic Whirl in Well-Aligned, Liquid-Lubricated End-Face Seals with Hydrostatic Tilt Instability," **25**(1), pp. 1–6.

[14] Etsion, I. and Constantinescu, I., 1984, "Experimental Observation of the Dynamic Behavior of Noncontacting Coned-Face Mechanical Seals," *ASLE Transactions*, Vol. 27, Paper No. 3, pp. 263–270.

[15] Green, I., 1989, "Gyroscopic and Support Effects on the Steady-State Response of a Non-contacting Flexibly Mounted Rotor Mechanical Face Seal," *Journal of Tribology*, Vol. 111, Paper No. 2, pp. 200–206.

[16] Lee, A. S. and Green, I., 1995, "An Experimental Investigation of the Steady-State Response of a Noncontacting Flexibly Mounted Rotor Mechanical Face Seal," *Journal of Tribology*, Vol. 117, Paper No. 1, pp. 153–159.

[17] Varney, P. and Green, I., 2018, "Dynamic modeling of an eccentric face seal including coupled rotordynamics, face contact, and inertial maneuver loads," *Proceedings of the Institution of Mechanical Engineers, Part J: Journal of Engineering Tribology*, Vol. 232, Paper No. 6, pp. 732–748.

[18] Norrbin, C. S. and Childs, D. W., 2018, "Predictions for Non-Contacting Mechanical Face Seal Vibration With External Excitation From Pump Vibration: Part II — Flexibly Mounted Rotor," *Volume 7B: Structures and Dynamics*, American Society of Mechanical Engineers, p. V07BT34A049, doi:10.1115/GT2018-77200.

[19] Norrbin, C. S. and Delgado, A., 2020, "A Novel Controlled-Motion Test Rig to Evaluate Effect of Synchronous and Subsynchronous Lateral Vibration on Reliability and Performance of Mechanical Seals in Pumps," *Volume 10A: Structures and Dynamics*, American Society of Mechanical Engineers, p. V10AT25A029, doi:10.1115/GT2020-15749.

[20] Childs, D., 2018, "A New Structural Dynamic Model for Pump Mechanical Seals Vibration Analysis Incorporating Squeeze Motion of O-Ring Seals and General Dynamic Motion of the Pump Housing and the Pump Shaft," *Journal of Tribology*, Vol. 140, Paper No. 6, p. 062201.

[21] Doğan, S., 2010, "Tribology and Dynamics of Engine and Powertrain," *Woodhead*.